Diploma Thesis

Building an Apparatus for Cold Rubidium Rydberg Atoms

Stephan Jennewein

August 22, 2012

5. Physikalisches Institut, University of Stuttgart, Germany

Abstract

The first part of this thesis covers the laser setup of a ^{87}Rb magneto-optical trap as well as stabilizing the lasers. Therefore a master-slave setup is introduced which utilizes two stabilizing techniques.
The second part of this work focuses on building a new computer aided control system for a new generation of National Instruments hardware.

Declaration

I hereby declare that this submission is my own work and that, to the best of my knowledge and belief, it contains no material previously published or written by another person, except where due acknowledgment has been made in the text.

Stephan Jennewein
Stuttgart, August 22, 2012

Contents

1 Introduction

Rydberg atoms have created a significant amount of interest in the last ten years [1], due to their unique properties which set them apart from ground state atoms and ions. Due to their large polarizability, they show strong long-range atom-atom interaction, only slightly smaller than the Coulomb-interaction between ions. But unlike ions, Rydberg atoms can be excited as well as de-excited in a controlled fashion by Rydberg excitation lasers, allowing one to turn on and off this strong interaction at will.
The usefulness of this flexible interaction has been recognized over ten years ago for its suitability to realize quantum gates with single atoms [2] as well as atomic ensembles [3]. Since then, a growing number of experiments have demonstrated these ideas: the Rydberg-Rydberg interaction has been observed in the form of excitation suppression due to the Rydberg-blockade effect in cold atomic ensembles [4, 5] as well as between pairs of single atoms [6, 7]. This has enabled the first demonstration of Rydberg based two-qubit quantum gates [8, 9]. More recently, the usefulness of Rydberg atoms for quantum nonlinear optics has been recognized. A ground-breaking first experiment in 2010 showed strong optical nonlinearities in a dilute cold Rydberg-gas [10]. This has by now been extended to the single photon level, showing strong nonlinear behaviour on the level of individual light quanta [11].

The 5th Physics institute, host institute for this diploma thesis, has been at the forefront of this exciting new field for many years. The existing Rydberg-BEC apparatus has produced a variety of spectacular results over the last years, including the first Rydberg excitation of a Bose-Einstein condensate (BEC) [5], universal scaling in the strong blockade regime [12], the observation of ultra long range molecules [13], and the study of Förster resonances in ultracold ensembles [14]. In parallel, a new research direction has been opened over the last years, implementing Rydberg-blockade physics with thermal atoms. In combination with state-of-the-art microfabrication [15, 16], this effort aims at the development of novel Rydberg-based sensors [17] and scalable Rydberg-quantum gate structures [18]. First proof-of-principle experiments showing coherent Rydberg-dynamics on the nanosecond scale [19, 20] demonstrate the feasibility of this promising approach.

Based on this vast experience with Rydberg-physics, in 2011 the construction of a second apparatus for Rydberg-excitation in BEC was begun. The main focus of this new setup is the combination of Rydberg-specific elements (precise electric field control, ion detection) with high resolution optics. The latter will enable both spatially resolved

preparation as well as detection of single, collective Ryderg-excitations (so called Rydberg superatoms). During this diploma thesis various aspects of the new design have been developed and optimized. The two main topics of this thesis are the setup of the laser system required for the initial magneto-optical trap and imaging of the ultracold atoms (section 3), as well as the realization of a completely new experiment control software to enable the synchronized control of over 100 digital & analog channels with microsecond precision to remote control all the various aspects of the new setup (section 4). Beyond these two subjects, this thesis contributed to the overall design and construction of the new setup. By incorporating the knowledge gained from the existing setup, a number of technical improvements could be made that facilitate highly stable Rydberg-excitation with fast repetition rate in this second-generation setup. An overview of the new setup and the realized improvements is given in section 2.

2 Setup Overview

As mentioned in the introduction, this newly designed experiment should fulfill various design criteria both for the initial production of ulta-cold atomic ensembles, as well as for the actual Rydberg experiments.
Large ultracold thermal clouds or even Bose-condensed ensembles (BECs) should be achievable with fast repetition rate, very good long-term stability, as well long, vacuum-limited lifetime. For the actual Rydberg-experiments high resolution optical access, efficient ion/electron detection, and extremely precise electric field control are the main goals.
In this chapter, an overview of the new setup and the planned experiment procedure is given, which will explain the general ideas to achieve all these design goals.
For practical issues this new experiment is split into two optical tables. One table is dedicated to the laser setup and the other one to the vacuum setup. With this decision it was possible to transport these tables with our regular elevator to the 5th floor where our experiment is housed. Furthermore, splitting the table gives more people the opportunity to work in parallel. Each table has a rack built around it, in order to store power supplies and measurement equipment.

2.1 Setup

For practical issues this new experiment is split into two optical tables. One table is dedicated to the laser setup and the other one to the vacuum setup. Splitting the table gives us an increased stability, as the vacuum equipment does not interfere with the sensitive laser electronics.

2.1.1 Laser

For the magneto-optical trap (MOT) we are using three diode lasers. These lasers are in a master-slave setup in which the master laser is frequency stabilized to a Doppler-free Dichroic Atomic Vapor Laser Lock (DAVLL) [21] and the two slaves are locked relative to the master with a frequency offset lock (FO-lock) [22]. Chapter 3 describes the master-slave setup in detail.
The Rydberg excitation is achieved by a two photon transition. Therefore one diode

laser[1] running at 780 nm and a second diode laser[2] running at 480 nm is used. Those two lasers are locked to an optical cavity with the Pound-Drever-Hall[23] method. This setup is described in Christoph Tresp's master thesis[24].

From this first table the laser light is guided via single-mode fibers to the vacuum table.

2.1.2 Vacuum Chamber

The second table is solely dedicated to the vacuum apparatus. One key point of this setup is the two-chamber approach separating the initial laser cooling area from the actual experiment area. Additionally, the experiment area is situated in a glass cell instead of the typical stainless steel chamber to improve optical access and minimize distance between atoms, optics, and detectors.
Inside the high pressure (approximately 10^{-9} mbar) chamber the MOT is loaded from the vapor pressure of rubidium. As the vapor pressure of rubidium is around 10^{-7} mbar at room temperature a valve has been installed to control the pressure. When the MOT is fully loaded the atoms will be transferred through the differential pumping stage into the low pressure chamber using a magnetic transport[25]. In the low pressure (approximately 10^{-11} mbar) chamber the Rydberg excitation takes place. Such a setup combines the benefits of a fast loading magneto-optical trap together with the ability of keeping the atoms trapped for a long time.

The setup is shown in figure 2.1. In the following subsections the setup is described according to the experimentation process.

[1] Toptica DL Pro
[2] Toptica TA-SHG Pro

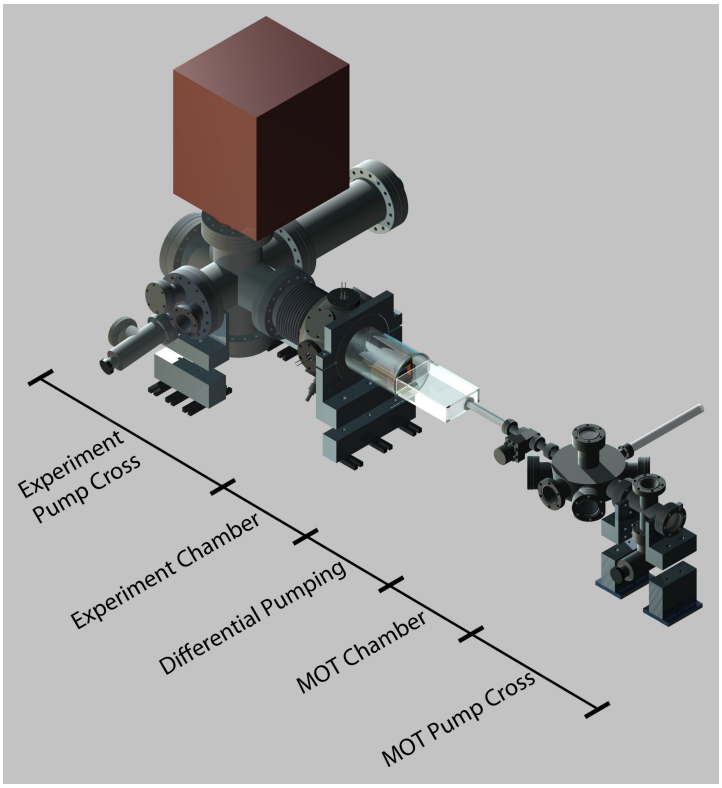

Figure 2.1: The vacuum chamber setup.

Magneto Optical Trap Chamber

A CAD drawing of our MOT chamber design is shown in Figure 2.2. The MOT chamber consists of a cylindrical body which has 10 flanges attached. 6 flanges have window mounts to shine in the laser light for the trap. The laser beams have a diameter of 3.8 mm. Using such large beams results in a big capture area for the MOT and fast loading rates. This enables the capture of $\sim 10^9$ atoms within 3 s.
On the back side a reservoir with 5 g rubidium is placed to have enough rubidium in stock for the next years. To keep the pressure at 10^{-9} mbar a valve has been installed between the reservoir and the chamber to regulate the rubidium pressure inside the chamber.
On the right-handside a pump-cross is attached, which has a valve to connect a turbo pump, and where a permanently running ion pump[3] is mounted to.
An ion gauge has been installed on the flange vis-a-vis of the reservoir to keep track of the pressure inside the chamber.
The valve on the left separates the Rydberg chamber from the MOT chamber. This is mostly for maintenance purposes, for the case that one half of the chamber has to be

[3]VARIAN Vacion Plus 75 Starcell

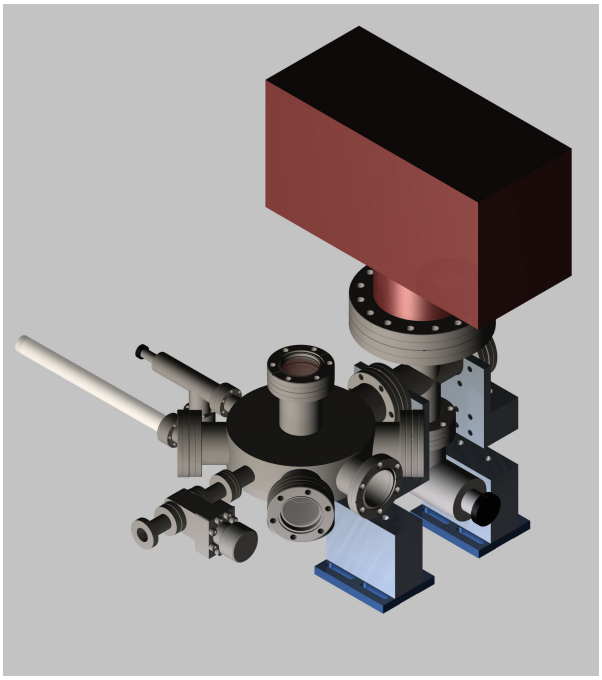

Figure 2.2: The schematic construction of the magneto-optical trap part of the vacuum chamber showing the MOT chamber in the middle. To the right a pump-cross is connected together with an ion pump. In the back of the picture the rubidium reservoir can be seen. To the left the valve separating the MOT and the Rydberg chamber is installed.

opened one can close the valve so that it is not necessary to evacuate the whole vacuum setup afterwards.

Magnetic Transport

After having loaded the MOT, the atoms are prepared by optical pumping into a low field seeking state. After the initial MOT phase, the temperature of the atoms is further reduced in a 10 ms phase of polarization gradient cooling. This is followed by a brief optical pumping phase which transfers all atoms into the $F = 2$, $m_F = 2$ Zeeman state, which can be trapped magnetically. At this point the MOT-coils are switched on again at much higher current to realize a quadrupole field with sufficient gradient to trap the atoms magnetically. Then the atoms have to be transferred into a magnetic trap.

In figure 2.3 our transport setup can be seen. The coils are glued into holders made out of aluminum using a thermal adhesive[4]. An exception are the 2 coils of the final Anti-helmholtz pair (green) and the perpendicular Ioffe coil (yellow). These 3 coils form

[4]EPO-TEK T7110

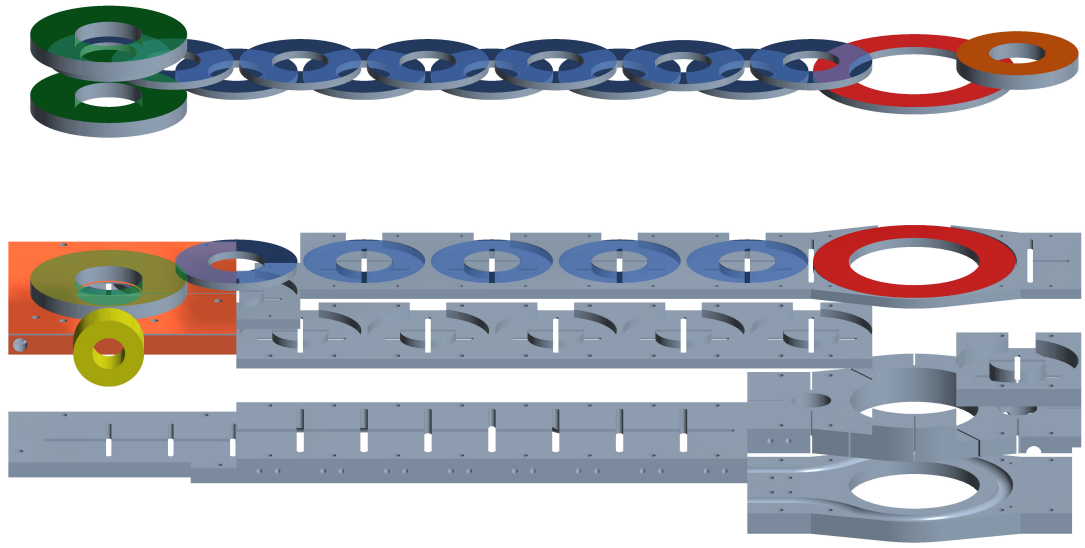

Figure 2.3: CAD drawing of the construction of our magnetic transport. All coils are glued into holders of aluminum or copper. Those holders are connected to a water cooled heat sink. The 16 blue and the one red coil pairs are in anti-Helmholtz configuration. The blue ones do the transportation and the red is for the MOT. The orange pair is in anti-Helmholtz configuration, too, but has a swapped polarity and creates an additional gradient in the transport direction. The lower orange coil is not shown here. On the left the inner green pair is in anti-Helmholtz configuration for the QUIC-trap while the outer green coil pair generates a homogenous offset field for mode matching in z-direction. The yellow coil is a Ioffe-coil which creates the non-zero offest field for our Quic trap.

the QUIC trap [26] which forms the end of the magnetic transport and holds the atoms during the actual experiment stage. There a current of about 40 A is being applied for up to one minute. To get rid of the large amount of dissipated heat they are placed into copper holders which are directly water cooled.
Transportation of the atomic cloud starts at the center of the red coil pair which provides the magnetic field for the MOT. At first the blue coils, close to the MOT, and the orange ones are ramped up. The orange coil pair functions as push coils to move the field zero from the MOT region along the transport axis. Without these coils there would be a strong deformation of the cloud during the first step when the atoms are handed from the larger MOT coils to the first transport coil pair.
To insure that the aspect ratio of the transported cloud stays constant over the whole

transport three coils have to be on at all times. With this pattern it is possible to transport the atoms from the MOT chamber to the Rydberg chamber. Arriving at the Rydberg chamber the atoms are transported around the corner into the QUIC-trap , which is produced by the green coil pair and the yellow Ioffe coil. As two green coil pairs can be seen, the outer one is in Helmholtz configuration to be able to move the atomic cloud into the focal plane of the lenses, which are focusing the laser beam inside the atomic cloud. The final trap location is not aligned along the transportation axis to minimize the disturbance of hot atoms traveling through the differential pumping stage on there own. For this reason the final trap is placed around the corner, as these atoms can leave the differential pumping stage only under a small angle.

Rydberg Chamber

Figure 2.4a shows the vacuum setup of the Rydberg stage. The experiments take place in the most right part, which is made out of pure glass[5]. This gives the possibility to fit in a science chamber, which enables good optical access along multiple axes at the same time.
Inside the glass cell a custom-made experiment (see figure 2.4b) cage will be installed. The center of the cage overlaps with the field minimum of the QUIC trap, so that the atoms are trapped inside the cage. This inserted cage serves as a Faraday cage to shield the Rydberg atoms from external electric fields. The 6 sidewalls of the cage are made out of titanium which has an exceptionally low magnetizability. Each of the 6 sides can be independently charged, which provides great flexibility in creating arbitrary electric fields for manipulating Rydberg atoms

Besides the high resolution of the ion detection, two aspheric lenses are embedded into the electrodes of the cage which are facing directly to the upper and lower walls of the glass cell. With these lenses we get a resolution of approximately 1 µm. A third lens with a resolution of 2 µm is mounted inside the Ioffe-coilt outside the vacuum.

Connected to the glass cell is an octagon, which has six feedthroughs attached. These feedthroughs are used to connect the two ion detectors to our measurement equipment as well as the six cage electrodes to the voltage supplies.
The next part of the vacuum setup is a pumping cross connected both to an ion pump[6] and a titan sublimator. These two devices are needed to keep the pressure in the Rydberg chamber at the lower end of 10^{-11} mbar. Furthermore a valve where we can connect an external turbo pump is mounted on the pumping cross. To measure the pressure inside of this part of the vacuum chamber a second ion gauge is attached, as well.

[5]Borosilicat, product name Tempax
[6]VARIAN Vacion Plus 150 Starcell

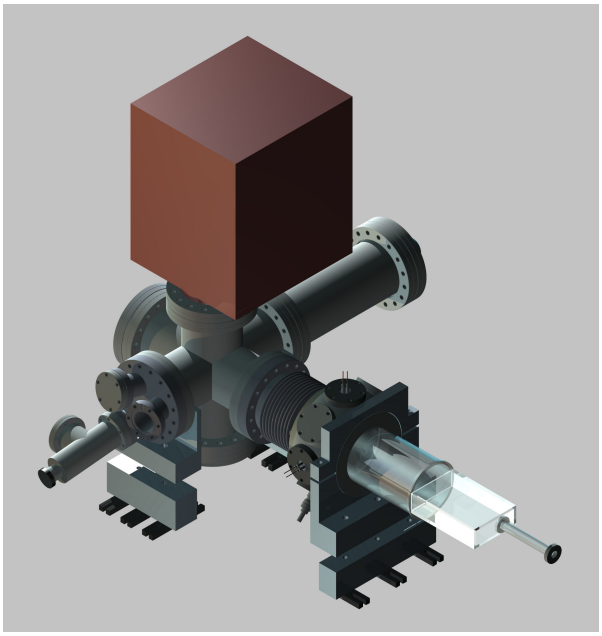

(a) Shows the setup of the experimentation stage. On the left the glass cell is connected to an octagon which holds the feedthroughs. Next to the octagon is the pump cross which has an ion pump and a titan sublimator connected. It also includes an ion gauge to measure the pressure as well as a valve to connect external pumps.

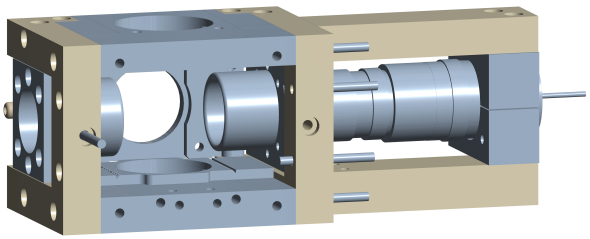

(b) The cage which is inserted into the glass cell. Each wall is made out of titan. These titan electrodes are separately addressable by a voltage of up to 2 kV. On the right the holder for the MCP can be seen.

Figure 2.4: a) shows the Rydberg chamber of the vacuum setup. b) shows the cage which is fit into the glass cell.

3 MOT Lasers & Optics

This chapter describes the laser setup used to realize the MOT in the new setup. In the course of this thesis active stabilization schemes for 3 diode lasers have been built and optimized. The achieved stability of the MOT lasers greatly exceeds the requirements set by the excited state lifetime.

3.1 Motivation

Building a setup for laser cooled atoms, having lasers with narrow bandwidth and very stable absolute wavelength is a necessity. The stability of free-running lasers is usually not sufficient for this purpose, as electrical and acoustic noise result in frequency fluctuations larger than the required stability. Consequently, active frequency stabilization techniques are employed.
We are using diode lasers from Toptica[1] running at 780 nm. Diode lasers have the advantage that their frequency can be modulated easily and rapidly. Additionally, they are small in size which saves space on the optical table and making a compact setup feasible.
Our diode lasers have two inputs for controlling the frequency. As the injection current is heating up the diode, which stretches the diode longitudinal cavity length. The piezo can change the length of the external cavity, which formed with a grating by retroreflection. If the piezo and the heating moves into the same direction it is possible to scan the laser over a large frequency range. Due to this, our diode lasers are mode-hop free tunable over a range of up to 50 GHz.
With the first control input the injection current can be controlled this results in a changed optical path length in the cavity. In fact a laser is working like a cavity, where constructive interference can only occur at certain frequencies. As a result the output wavelength of the diode laser changes.
The second modulation input is for controlling the grating mounted on a piezo. This grating builds an external cavity with a higher free spectral range. By moving the piezo the frequency can be tuned. As the fed back light travels through the active region of the diode again, the process of enhanced stimulated emission is repeated for this wavelength and ends up in a higher power output.

This chapter describes the basics of control theory and how stabilizing has been done

[1] DL Pro and TA Pro

with a master-slave setup. The master laser has been locked to a DAVLL spectroscopy and the slave lasers have been locked with a FO-lock relative to the master laser.

3.2 Feedback

3.2.1 Control Theory

To stabilize a laser to a specific frequency, one has to measure the deviation of the actual output frequency from this set point and turn this difference into an (ideally linear) error signal with a zero crossing at the set point. A controlling device, which uses this error as an input and feeds back onto the laser is then used to actively correct the output frequency. The mathematical framework for the description and optimization of such feedback loops is called control theory. The relevant aspects for our laser stabilization are discussed in the following.

In general, the behaviour of an open or closed feedback loop or of single components of the loop can be written in the time domain. This results in differential equations for the feedback loop. It is extremely convenient instead to work in the frequency domain, by performing a Laplace transformation.

$$y(s) = \int_0^\infty y(t)e^{-st}dt, s \in \mathbb{C}$$

This turns the differential equation into an algebraic one, which is usually much more intuitive. Now a descriptive way is shown to gain the transfer function in frequency space:

For a linear system shown in figure 3.1 and in the absence of noise, a system is described by its response function:

$$Y(s) = W(s) \cdot G(s)$$

Where $Y(s)$ is the input, $G(s)$ is the response function and $W(s)$ is the desired output.

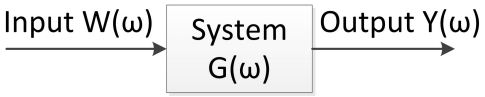

Figure 3.1: Response of a linear system

For example, in our case the system under consideration is the diode laser, which receives an input signal on the current modulation input. This in turn results in a change of the output frequency of the laser, as discussed above. For an ideal system without noise, where the transfer function is perfectly known, this control would be sufficient, as one can always achieve the desired frequency. In reality, though, no signal comes without

noise, so the presence of noise can be described by adding a disturbance. This leads to an error at the output with respect to the desired output. To compensate this error a controller is added with a negative feedback (see figure 3.2).

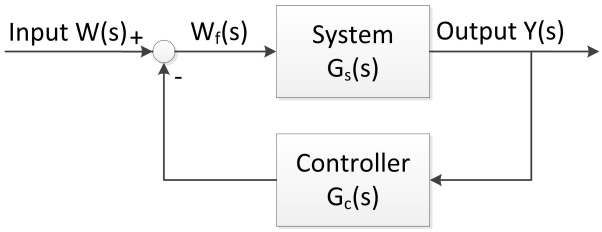

Figure 3.2: Block diagram of a closed loop

With this the transfer function is given by:

$$Y(s) = G_s(s) \cdot W_f(s) \Rightarrow W_f(s) = \frac{Y(s)}{G_s(s)}$$

$$W(s) - G_c(s) = W_f(s) = \frac{Y(s)}{G_s(s)}$$

$$\Rightarrow W(s) = Y(s) \cdot \frac{1 + G_s(s) \cdot G_c(s)}{G_s(s)}$$

$$\Rightarrow \frac{Y(s)}{W(s)} = \frac{G_s(s)}{1 + G_s(s) \cdot G_c(s)}$$

We define the open loop transfer function as:

$$G_{open}(s) = G_s(s) \cdot G_c(s) = \frac{Y(s)}{W(s)}$$

and the closed loop as:

$$G_{closed}(s) = \frac{G_s}{1 + G_{open}}$$

As the transfer function is a complex value it cannot be measured directly. What can be measured is the gain which is $|G(s)|$ and the phase which is the argument of $G(s)$ namely $s = i\omega$.
To visualize these two values it is common to do a Bode plot. A Bode plot is a graph of the transfer function, plotted with a log frequency axis. It is a combination of a phase plot and a magnitude plot which represents the gain of the system.

3.2.2 PID Controller Basics

As described in the control theory section 3.2.1 a controller is needed to compensate the residual error. One possibility to realize a controller is a so called PID controller. Although it benefits from its simplicity, the performance as a controller is quite convincing. Such a PID controller as the name implies consists of three terms, proportional, integral and derivative, respectively. The ideal transfer functions of these terms are defined as follows:

Name	Transfer function	Bode plot
P	$G_P(s) = K_P$	see figure 3.3a
I	$G_I(s) = \frac{K_I}{s}$, K_I is a amplification constant	see figure 3.3b
D	$G_D(s) = K_D \cdot s$, K_D is a amplification constant	see figure 3.4a
PID	$G_{PID}(s) = K_P(1 + \frac{K_I}{s} + K_D \cdot s)$	see figure 3.4b

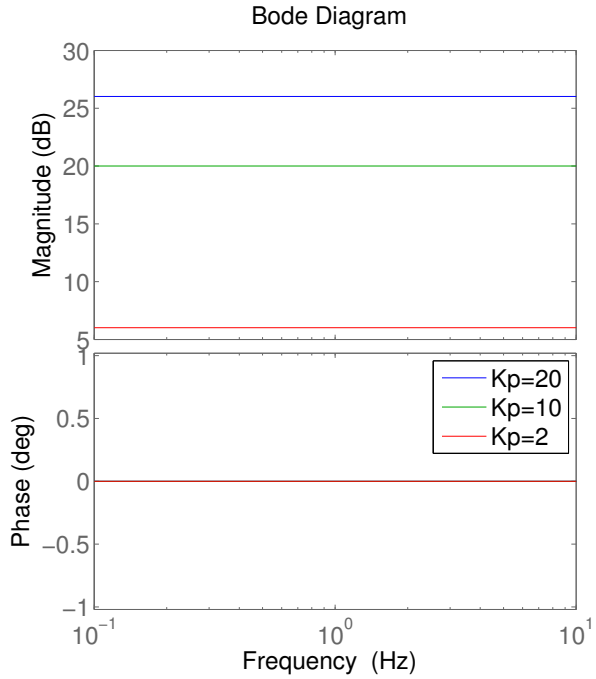

(a) Transfer function of the proportional part.

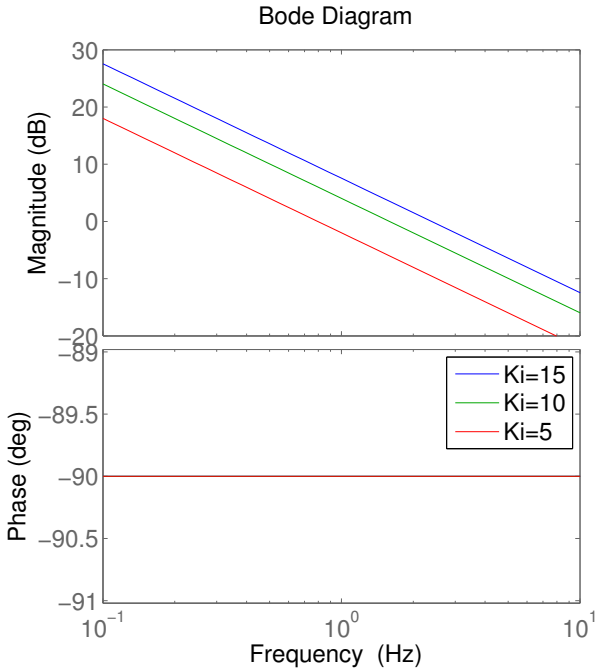

(b) Transfer function of the integral part.

Figure 3.3: Transfer function of the proportional and integral part.

The proportional term adds only a constant gain without changing the phase at all frequencies. The integral term works only on low frequencies as the gain drops exponentially with higher frequencies. This term also adds a $-90°$ phase shift. In contrast, the derivative term acts only on fast changes in other words high frequencies and adds a 90° phase shift to the signal. Combining all three terms yields a PID controller.

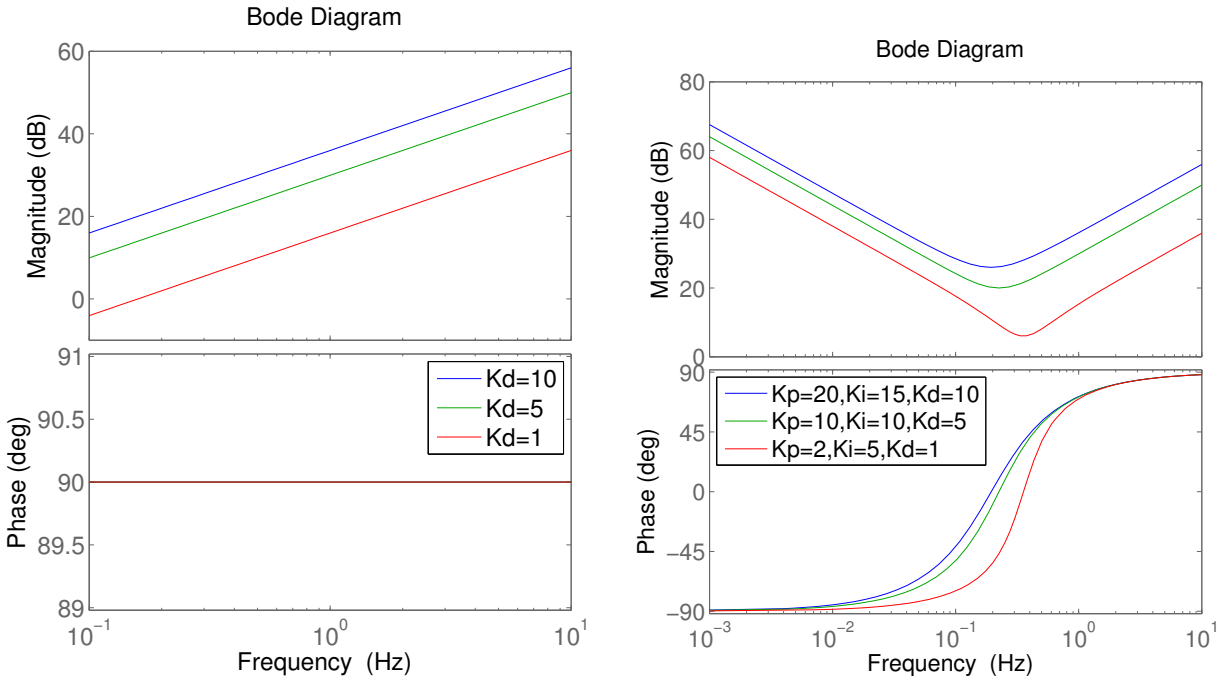

(a) Transfer function of the derivative part.

(b) Transfer function of a PID controller.

Figure 3.4: Transfer functions of the derivative part and the whole PID controller.

As part of this thesis, a new PID controller has been designed and tested. This includes the development of the schematics and the realization of an actual board layout, using the electronics design software EAGLE. A printed circuit board of the completed design was then printed by the company PCB pool.

This PID board was explicitely optimized for the stabilization of our diode lasers, directly implementing 2 output paths for the current and piezo modulation. The bandwidth of each of these paths was optimized for the respective bandwidth of current and piezo modulation.

While laser frequency stabilization is the main purpose of this design, the resulting PID controller can be used in any other feedback loop, as it provides a general implementation of the control theory discussed above. For example, the design I developed has since been used also for intensity stabilization of our lasers [27].

As our lasers have two input connections one for modulating the injection current and the other one for modulating the grating mounted on a piezo, our PID controller needs two output connectors. The output for the current modulation has the full bandwidth

of our PID controller which is up to 1 MHz. For the piezo modulation a low pass is added to the signal path to avoid mechanical resonances.
Another important detail was to keep the signal path on the board to reduce noise effects. For that reason all BNC connectors are double connectors and attached directly on the board. Additionally, the switches to turn on the controller are connected to a digital switch which is socket mounted. With this the front panel is decoupled from the signal path.

We are using the operational amplifier OP467 for this board. This is a quad packaged, precision, high speed op-amp with a stable open-loop response function. Figure 3.5 shows the circuit for the PI controller. As we tried to save op-amps to minimize the phase shift each of them adds to the signal, the proportional and integral terms where combined in one op-amp. In this setup the op-amp output voltage is given by:

$$U_o = -U_i \cdot \frac{1}{i\omega C_{36} \cdot R_{48}} \cdot \frac{R_{49}}{R_{48}}$$

The resistors R_{15} and R_{18} are for impedance matching with the derivative term.

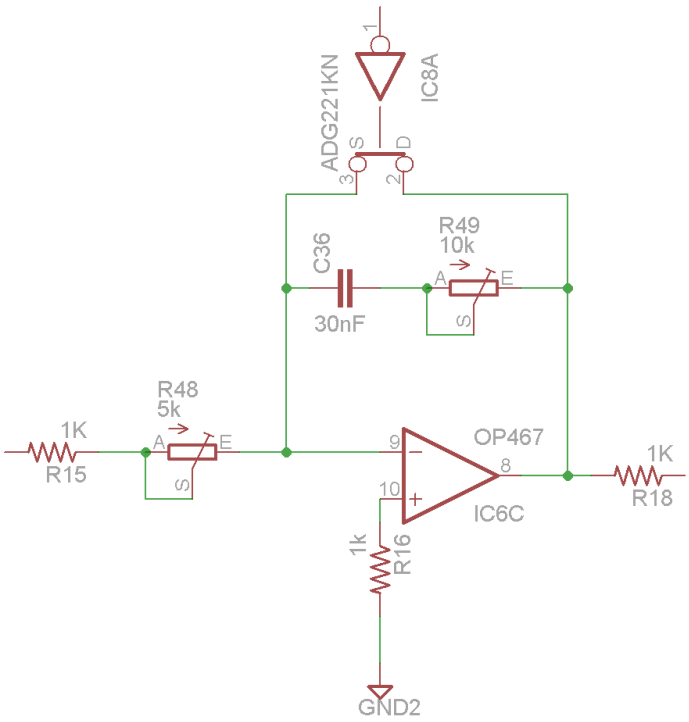

Figure 3.5: Op-amp configuration for our PI controller.

The ADG221KN is the mentioned digital switch. This switch is connected to a mechanical counterpart and follows its position. For disabling the PI controller it is important

to shorten it. Otherwise the integral part would start summing up and if the switch closes the controller would not lock at the desired position, because the accumulated gain of the integral term would be too high. Figure 3.6 shows the derivative term of our controller. The output voltage is described as:

$$U_o = -R \cdot C \cdot \frac{\mathrm{d}U_i(t)}{\mathrm{d}t}$$

R_{43} and R_{20} are again for impedance matching. The derivative part has an own switch to select whether this controlling component is needed or not.

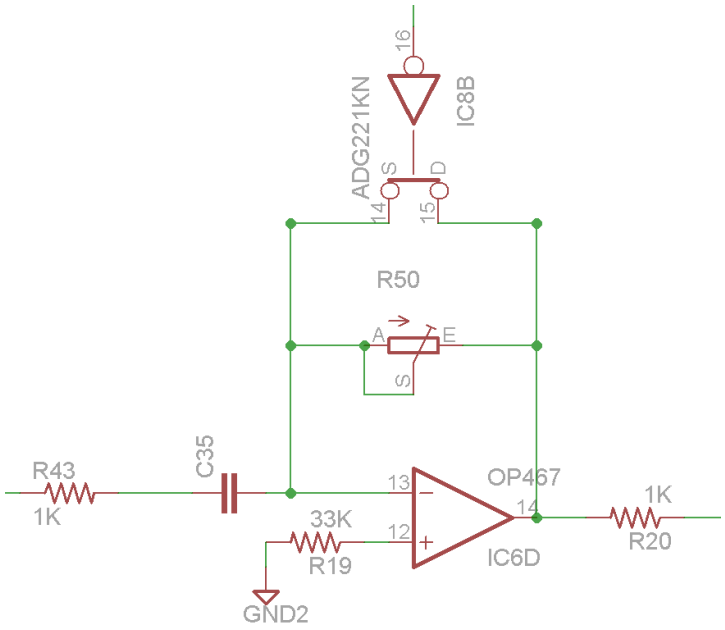

Figure 3.6: Op-amp configuration for D controller.

After the two controller the signal is summed and distributed to the two outputs. Each output has an extra inverting stage where the signal can be inverted to lock to the right slope sign. Additionally, the piezo output has the possibility to be attenuated relative to the current output. Due to the different amplification behavior this is often necessary.

The PID board is getting its power from a switching power supply[2]. With this each PID controller is galvanically decoupled from each other. The switching power supply is then fed into a series voltage regulator one for the positive and one for the negative voltage to get rid of any ripple the switching power supply is adding to the direct-current (DC).

[2]Traco TEN5-1223

3.2.3 Stability Criteria

Only a negative feedback system can be stable, since in a positive feedback disturbances would be amplified. Still, even a negative feedback can be unstable. This can be directly seen from the expression for the closed-loop gain. Since the quantities are complex, the denominator can become zero, which results in infinite gain at specific frequencies, so called poles.

There are two criteria to name phase margin and gain margin.
In an electronic amplifier, phase margin is the difference between 180° and the phase measured in degree, as a function of frequency, when the gain crosses unity. Looking at a negative feedback, a zero or even negative phase margin, when the gain exceeds unity, guarantees instability. Having a positive phase margin a proper operation is ensured. In practice, feedback amplifiers may not reach a phase margin of 0°. Many practical factors reduce this margin below the theoretical minimum. A prime example is a capacitive load connected to the amplifier. Therefore a minimum of 45° is a good value for applications [28].

An equivalent definition to the phase margin is the gain margin. Gain margin is defined as the difference of unity gain and the gain measured, as a function of frequency, when the phase crosses $-180°$.

3.3 Error Signal Generation Schemes

3.3.1 DAVLL spectroscopy

As a free running laser without frequency stabilization fluctuates too much, due to electronic and acoustic noise, to use it for a magneto-optical trap, it has to be locked to a frequency reference. For this reason the master laser is locked onto a DAVLL signal [21]. This signal is generated by having two counter propagating laser beams guided through a rubidium cell shown in figure 3.7a. In this setup the same beam is used for pumping and probing as the beam travels through the cell, the first time it is the pump beam and on its way back due to the intensity loss it is the probe beam. Sub-Doppler resolution is reached because only atoms moving slow enough (the Doppler shift has to be in the same order of magnitude as the natural linewidth) interact with both, the pump and the probe beam. The pump beam reduces the amount of ground state atoms with which the probe beam can interact by optical pumping. Regarding the selection rule of $\Delta F = 0, \pm 1$ three resonances are expected, but also crossover resonances can be observed between two expected resonances.
To lock an arbitrary system an error signal with zero crossing is required. The transition, where the σ^+ or the σ^- component of the probe beam is resonant, is detuned because of the Zeeman shift, which is induced by an external magnetic field. Measuring the two

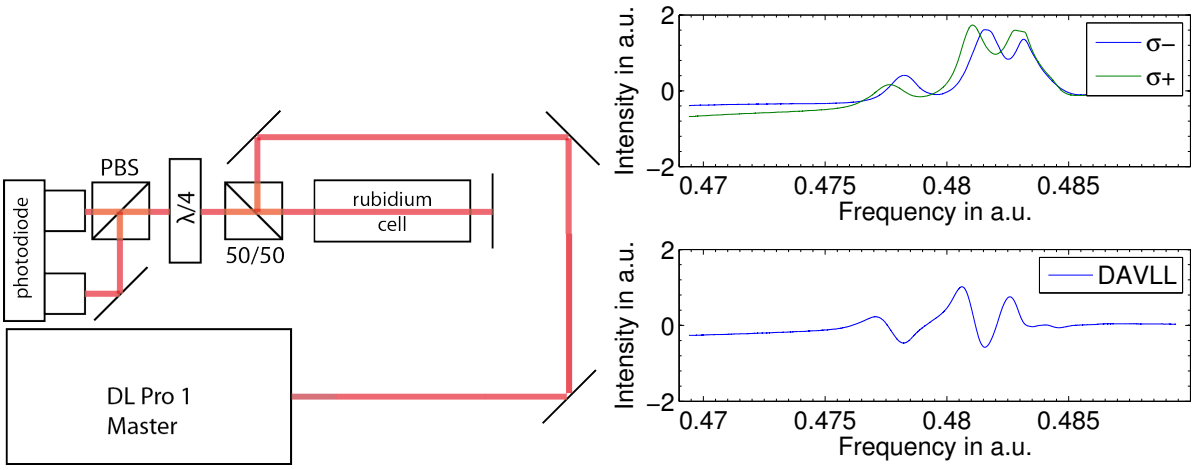

(a) Setup for DAVLL spectroscopy

(b) DAVLL spectroscopy signal

Figure 3.7: Setup and signal of the DAVLL spectroscopy

polarization components of the light results in the green and red Doppler-free curves in figure 3.7b. Subtracting these two slopes from each other the DAVLL signal (blue) can be seen. The DAVLL slope should have its zero crossings where both curves crosses each other. This is not the fact due to some electronic offset, but can be compensated.

With this method we are locking our master laser to an atomic reference which in our case is the crossover resonance of $^{85}\mathrm{Rb}(3 \rightarrow 3)(3 \rightarrow 4)$ which is at 780.244 nm

3.3.2 Frequency offset lock

The FO-lock is a method to lock a second laser relative to a reference laser [22]. Therefore two laser beams with low intensity are beat and measured with a photo diode. The measured signal is fed into a delay line box where the beat signal is mixed down with a radio frequency from a voltage controlled oscillator (VCO). After mixing the signal down, it is fed into an interferometer where one branch is delayed and then interfered with the other branch. A schematic setup can be seen in figure 3.8.

Assuming laser light as a monochromatic, plane wave a delay-line the signal measured on the photo diode is the intensity of the two combined beams, which includes various interference terms:

$$V_{PD} \propto \cos(\omega_m t)+\cos(\omega_s t))^2 = 1+\frac{1}{2}(\cos(\omega_m t)+\cos(2\omega_s t))+\cos((\omega_m+\omega_s)t)+\cos((\omega_m-\omega_s)t)$$

where ω_m is the frequency of the master laser and ω_s the frequency of the slave, $\omega_b = |\omega_m-\omega_s|$ is the beat frequency. The DC voltage term is filtered out by capacitive coupling

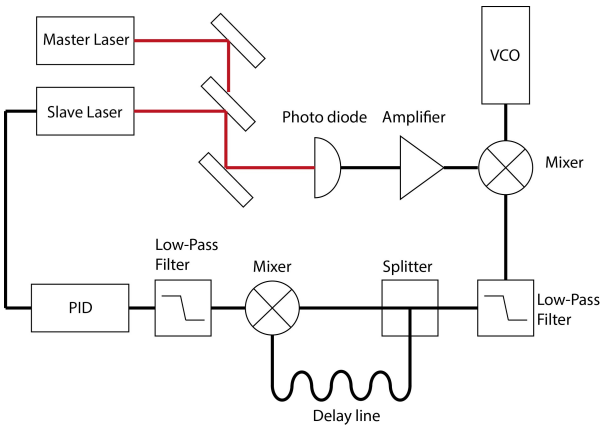

Figure 3.8: Schematic of the frequency offset lock.

of the photo-diode. The terms which are oscillating at higher frequencies cannot be detected by the photodiode and vanish automatically. The resulting beat frequency is then mixed with the output of the voltage controlled oscillator. This mixed signal can be written as a sum and a difference of frequencies $\omega_{\pm} = |\omega_b \pm \omega_{VCO}|$, where ω_{VCO} is the frequency of the VCO.

$$\cos(\omega_b t) \cdot \cos(\omega_{VCO} t) = \frac{1}{2}(\cos(\omega_b t + \omega_{VCO} t) + \cos(\omega_b t - \omega_{VCO} t)) \propto \cos(\omega_+ t) + \cos(\omega_- t)$$

To get rid of the sum term a low pass filter is installed. The remaining signal is split into two parts. One travels through a delay-line with length l and the other one is connected directly to a mixer, where both signals are mixed. The frequency of both components are the same, but the phase of the one coming out of the delay-line has a phase-shift of $\frac{l}{c}$, where c is the signal speed in the cable. The result after mixing both signals is given by:

$$V_{mix} = \cos(\omega_- t) \cdot \cos(\omega_-(t + \frac{l}{c})) \propto \cos(w_- \frac{l}{c}) + \cos(2\omega_-(t - \frac{l}{2c}))$$

Again a low-pass filter gets rid of the time dependent term. With this the result of the delay-line box is:

$$V_{out} \propto \cos(\omega_- \frac{l}{c}) = \cos((\omega_b - \omega_{VCO})\frac{l}{c})$$

This result is not time dependent anymore, but oscillates with $\omega_b - \omega_{VCO}$. As the cosine can be assumed to be nearly linear around zero this gives a good locking signal. Depending only on $\omega_b - \omega_{VCO}$ the lock point can be moved by changing the applied voltage to the VCO. With this it is possible to tune the locked laser. One can easily see that this concept is a little bit different from the DAVLL-lock, where the laser frequency

is directly locked to a reference. The FO-lock instead locks the relative frequency (beatnote) to a radio-frequency reference.

In our case the delay-line boxes have been built with standard components from Mini-Circuits. A simple scheme of the assembly can be found in the appendix in figure 6.1 for the 1 GHz beatnote and in figure 6.2 for the 5 GHz beatnote.

For detetection of the beatnote a fast photodiode[3] is used which is biased and amplified. Then this signal is fed into a beatnote box.

Parts of the 1 GHz beatnote box

Part Number	Component Name
ZX60-6013E-S+	16 dB Amplifier
ZFDC-10-5-S+	Directional Coupler
ZFM-2000+	Mixer
VAT-10+	10 dB Attenuator
ZX95-2150VW-S+	VCO
ZJL-3G+	Amplifier
ZFRSC-42-S+	Splitter
ZFM-2000+	Mixer
SLP-2.5+	Low Pass Filter

Parts of the 5 GHz beatnote box

Part Number	Component Name
ZX60-8080E-S+	8.5 dB Amplifier
ZFSC-2-10G+	Splitter
ZFMX-10G+	Mixer
VAT-10+	10 dB Attenuator
ZX95-5400-S+	VCO
ZJL-3G+	Amplifier
ZFRSC-42-S+	Splitter
ZFM-2000+	Mixer
SLP-2.5+	Low Pass Filter

The frequency range for the input signal from the photodiode depends on the used components e.g. VCO, low pass filter and mixer. Standard components are able of handling beatnote frequencies between a few MHz up to 5 GHz. The bandwidth of a delay-line is ca. 1 GHz. In our case we need one at 1 GHz and another one at 5 GHz. The 1 GHz beatnote is used for our cooling laser and the 5 GHz is used for the the repumper, for details see the MOT section 3.4.2.
It is possible to lock to any slope with the right sign. For this reason a spectrum analyzer is used to visualize the offset of the beatnote. Though a spectrum analyzer helps to find the right slope it is still possible to lock to the wrong frequency. To pay attention to this fact one has to check the absolute wavelength of the laser as the beatnote looks the same for an offset of ± 1 GHz. To decide between this two cases a wavemeter can be used which has a high enough resolution to differentiate between those two offsets.

The resulting error signal of a delay-line is shown in figure 3.9. Obviously the practical slope does not look like a cosine function. This is due to the low pass filters as they are adding ripples to the signal which are mixed, as well. Besides this, the overall electronic noise contributes to the deformation of the ideal cosine. Nevertheless, the steep slopes can still be used for laser locking as they are practically linear.

[3] Hamamatsu G4176-03

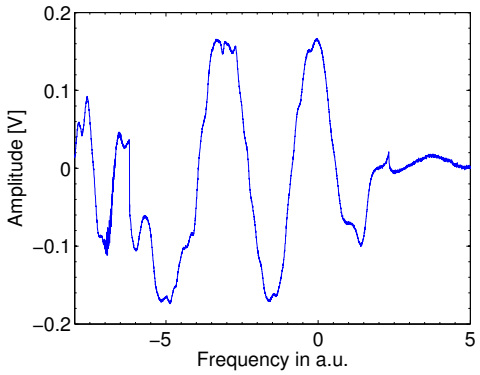

Figure 3.9: Error signal of a 1 GHz beatnote box, when the slave laser is scanned.

3.4 Implementation

3.4.1 Table Setup

As described in the overview chapter our setup is divided into two tables. One table is dedicated to the vacuum setup and one to the laser setup.
In figure 3.10 our setup of the laser table is shown. Starting at the top of the picture the master laser[4] which is frequency locked to a DAVLL spectroscopy at 780.244 nm can be seen. The beam of this laser is distributed to all the other lasers to be beat with them. Therefore one beam axis is traveling across the table. At the end the beam of the master laser is coupled into a fiber to have the possibility to use it elsewhere as a reference.
The second laser[5] is for imaging purposes, locked at 780.246 nm. One branch of the beam is beat with the master laser. The other one is going through a telescope into an acousto optic modulator (AOM) and is then coupled into a single mode fiber and guided to the experiment. The telescope in front of the AOM has the purpose of shrinking the beam diameter that the AOM can switch faster as well as having better coupling efficiency into the AOM.
The third laser[6] is the repumper, locked at 780.233 nm. The setup for this laser is the same as for the second one.
The forth laser[7] is the cooler locked at 780.246 nm, this laser consists of a seeding laser and a tapered amplifier. Again the laser beam is beat with the master beam and the laser beam is amplified up to ≈ 1 W. The amplified beam is then focused into an AOM and afterwards coupled into a single mode fiber. Focusing into the AOM again is for performance issues. The fiber is guided to the vacuum table.

[4]Toptica DL Pro
[5]Toptica DL Pro
[6]Toptica DL Pro
[7]Toptica TA Pro

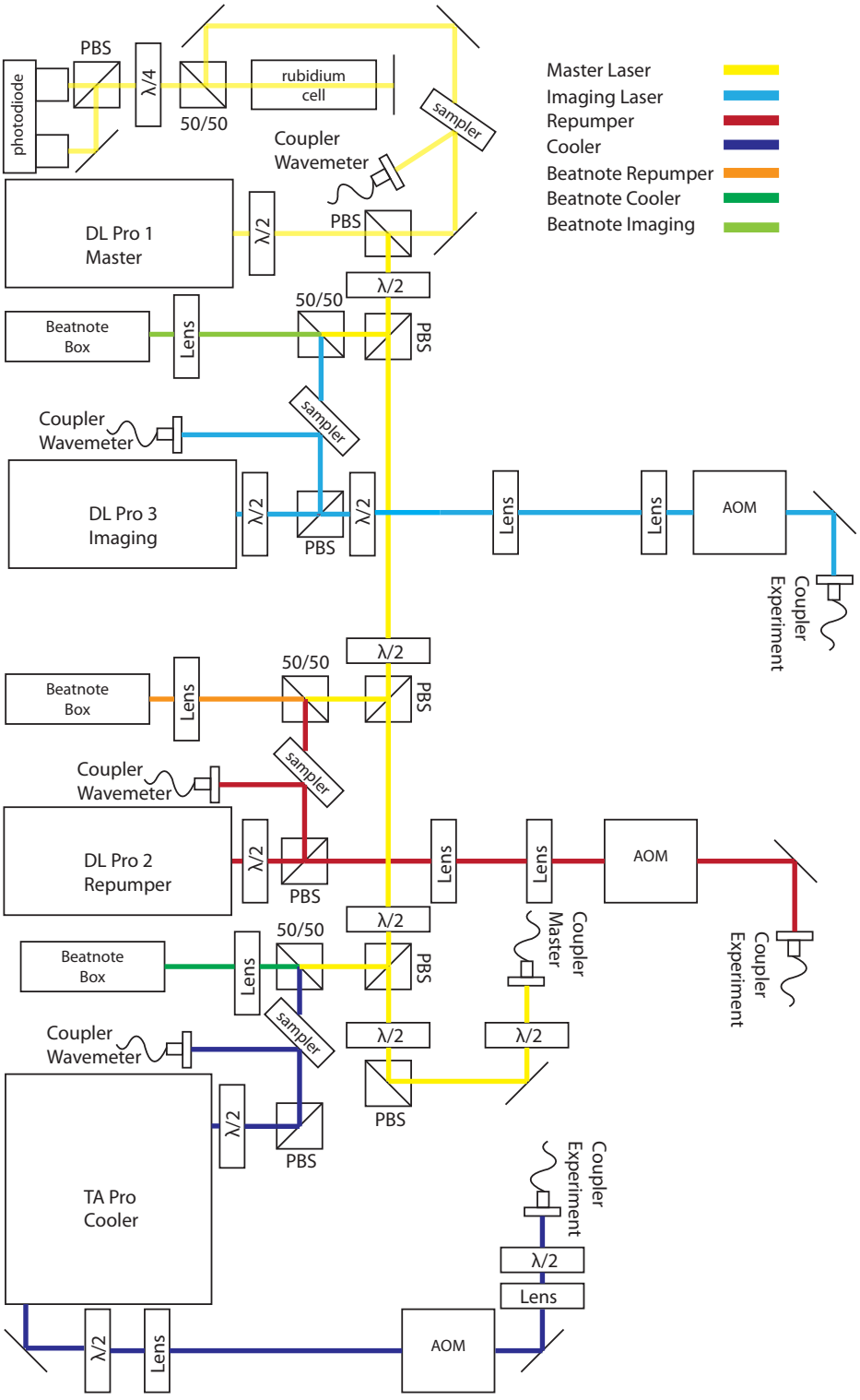

Figure 3.10: Schematic laser table setup

3.4.2 Magneto Optical Trap

For cooling rubidium atoms in a MOT, we are using a common scheme [29] for this element. As for cooling a closed transition cycle is needed. We are using the $5S_{1/2}, F = 2$ to $5P_{3/2}, F' = 3$ transition of ^{87}Rb. Slightly red detuned light is used, according to the $F = 2 \rightarrow F' = 3$ transition, to push the atoms into the center of the trap. Moreover the atoms have a little chance being excited to the $F' = 2$ state, from where they can decay into $F = 1$. In this dark state they do not interact with the cooling light due to the hyperfine splitting of 6.8 GHz and as a result are out of the cooling cycle. Therefore a repumper is used to pump atoms from $F = 1 \rightarrow F' = 2$ from where they can decay back into $F = 2$. With this scheme a closed cycle is reached.
In our scheme the cooler and repumper are not locked exactly at the frequency of the transition. This results from the frequency shift the AOM is adding, which has to be subtracted from the lock point frequency.

Laser	Transition	Frequency	Locked Offset
Master	$(3 \rightarrow 3)(3 \rightarrow 4)$	780.244 nm	0 Hz
Repumper	$1 \rightarrow 2$	780.233 nm	5.421 GHz + 80 MHz AOM
Cooler	$2 \rightarrow 3$	780.246 nm	1 GHz + 80 MHz AOM

Shown in section 3.5.2 our lasers are locked with a line width < 40 kHz. This is 100 times better than what is needed for our rubidium MOT since rubidium 87 has a natural line width (FWHM) of approximately $2\pi \cdot 6$ MHz [30].

3.5 Results

3.5.1 Transfer Function

Transfer functions and closed loop gains are measured with so-called network analyzers. Simplified, such an analyzer consists of a sweepable frequency generator and an oscilloscope. In our lab, we use a cheap commercial computer aided combination of these which already includes the required software.
Figure 3.11a shows the basic measurement configuration. The computer program scans the frequency of the sine wave with a constant amplitude. With one channel of the oscilloscope the output of the function generator is measured as a reference signal and with the second channel the output wire of the connected system is measured. The oscilloscope then compares the two signals and calculates $\Delta\phi$ and $Gain$ as shown in figure 3.11b.

This measurement setup has been built with a computer aided oscilloscope[8] and a com-

[8] Welleman PCS500

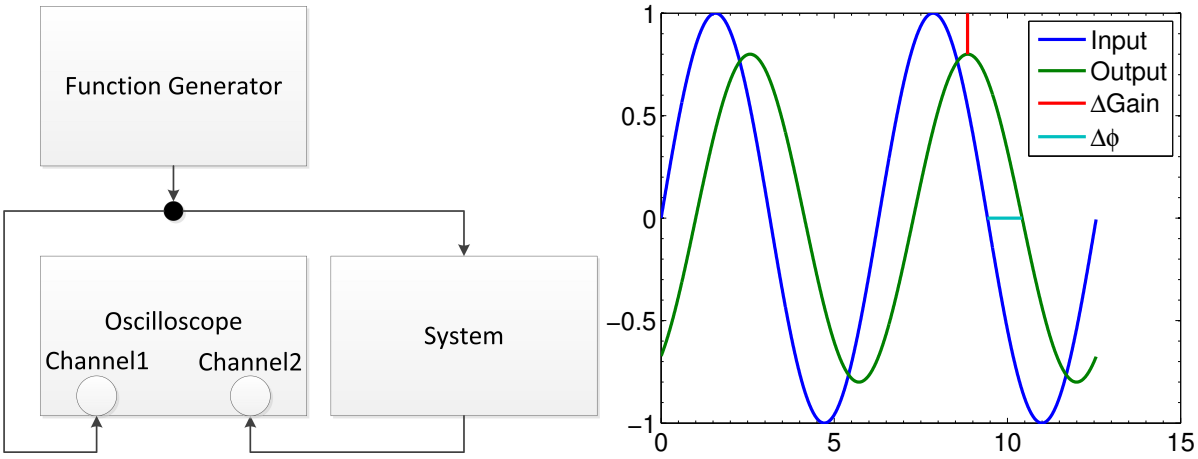

(a) Setup of transfer function measurement. (b) Comparing reference signal to measured signal.

Figure 3.11: a) show the schematic setup for measuring transfer function. b) shows the working principle of the software.

puter aided function generator[9]. To measure the transfer function of the piezo the output of the function generator has been set to 0.1 V_{pp} and a 1/320 attenuator has been used for the input signal. For the current it was measured with the same attenuator and 2.5 V_{pp} for the input signal. The measured transfer function for the piezo is shown in figure 3.12a and the one for the current is in figure 3.12b. The fluctuations in the diagrams are due to the measurement procedure and not actually part of the transfer function. As it can be seen in figure 3.12a the piezo has a resonance at 6.6 kHz. Toptica specifies the first resonance to be above 4 kHz which they fullfil. We apply a low-pass filter to the piezo output of our feedback controller that we never will reach this resonance. What can also be seen from the transfer function is that the feedback controller has to attenuate the transfer function because the one shown in these figures are not stable by the meaning of phase margin.

3.5.2 Lock quality

To check how good our lasers are locked we measured the error signal in closed loop configuration. The error signal represents the difference between the measured signal and the set point. That means, if a signal close to zero is measured the controller is doing a good job keeping the laser near the set point. First a reference curve with disabled controller was measured. Then the controller has been optimized and then measured. The result can be seen in figure 3.13a. The plot shows nicely that until 100 kHz the system is well controlled as the error is attenuated up to 30 dB. Afterall this is a good

[9]Welleman K8016

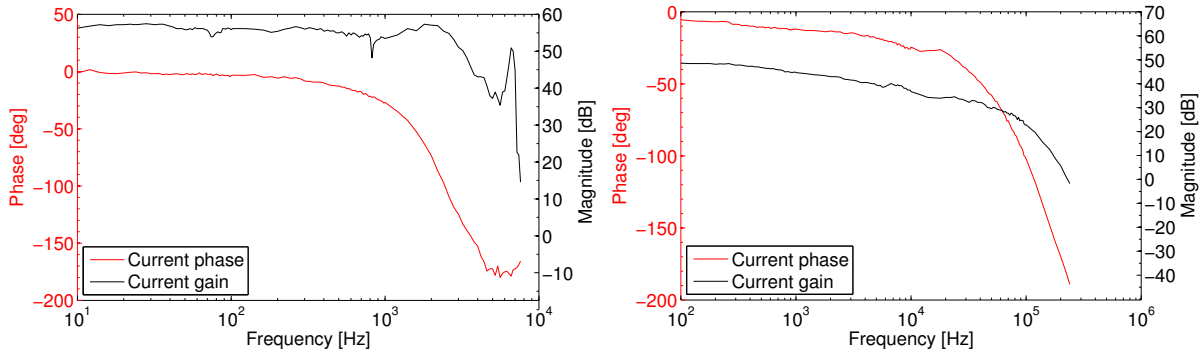

(a) Transfer function of the piezo.

(b) Transfer function of the current.

Figure 3.12: Transfer functions of the master laser.

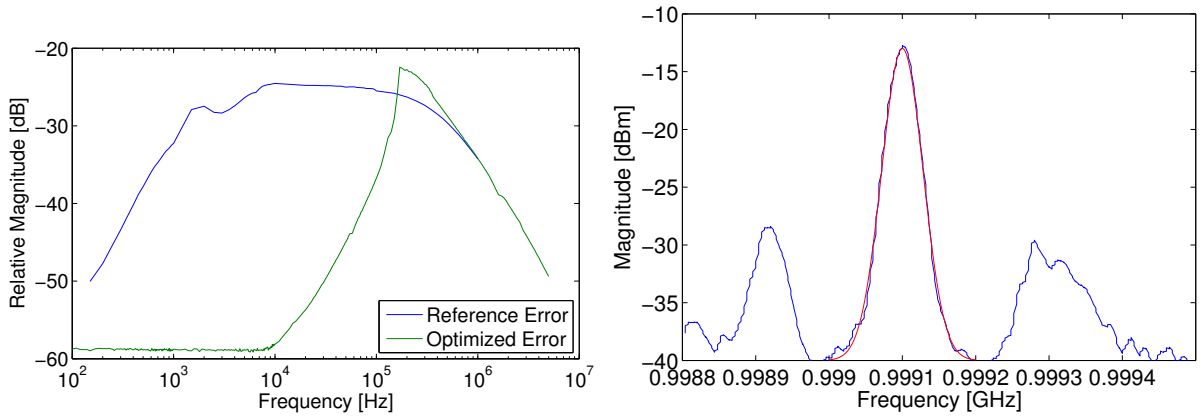

(a) Reference and optimized error function

(b) Spectrum analyzer signal for an optimized feedback controller.

result, because all acoustic noise (10 Hz to 20 kHz) as well as electronic noise of up to 100 kHz is very well attenuated.
At 200 kHz the error of the optimized controller exceeds the reference. This means that there the error will be amplified. This can be nicely seen with a spectrum analyzer (see figure 3.13b). The central peak is the locked beatnote at 1 GHz and an FWHM of 40 kHz. With this beatnote line width a upper limit for each laser line width is given. What can also be seen are two side-peaks, which have the exact distance to the central peak of 200 kHz.

3.5.3 Common Mistakes

First to mention our controllers have two outputs, each output can be inverted separately, to ensure the correct slope of the feedback loop for each arm. To find the right setting it is convenient to lock the laser with each output on its own. With this it should

be possible to find out on which slope sign which output is locking. Though speaking about slope sign the sign is only well defined with respect to some external parameters. In order to see the slopes either of the DAVLL spectroscopy or the offset-lock it is necessary to frequency scan the laser. A laser is scanned by applying a triangular voltage to the piezo actor. This is the reason why a rising slope of the spectroscopy on the rising scan function turns into a falling slope on the falling scan function. Another factor is the setting of the quarter-waveplate, after the DAVLL spectroscopy (see section 3.3.1), which could be randomly twisted. As the two saturation spectroscopies are subtracted from each other a 90° twisted waveplate changes the subtrahend and minuend. That leads to an inverted slope. All of these effects let appear the controller to be broken, but have to be checked to be sure.

Besides locking on the wrong slope it also possible that the error signal for an FO-lock, which can be monitored with an oscilloscope, is very small, but looking at the spectrum analyzer reveals the picture shown in figure 3.13. Comparing this with a well locked beatnote figure 3.13b higher harmonics of the feedback resonance can be seen. To get rid of those higher harmonic oscillations the gain of the feedback controller has to be reduced.

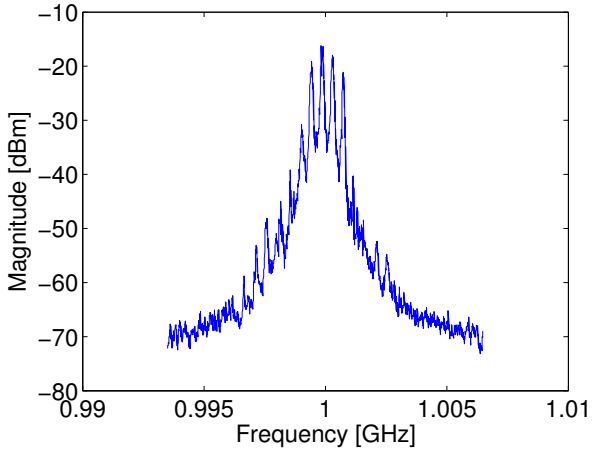

Figure 3.13: Spectrum analyzer signal for a lock with too much gain.

4 Computer Control

4.1 Motivation

For an experiment of this complexity a large number of devices has to be controlled synchronously, for example power supplies, shutters, AOMs. Already, for the magnetic transport 16 digital and 4 analog channels are used. As one example, for each FO-locked laser, one analog channel is needed to control the laser frequency by changing the VCO output, as well as two digital channel to control an AOM and a mechanical shutter for turning on and off the output beam. Therefore a computer aided control system is needed.
Besides the vast variety of channels the precision and speed is also an issue. The precision of such a system is divided into two parts. The first is the relative jitter between the channels which should be minimized by synchronizing the output signals. The second is the absolute time resolution of each channel. Additionally, the analog channels should have minimum of noise, as any residual noise can translate into jitter of actual experiment parameters. For example, noise on the VCO control voltage for the FO locks directly results in frequency jitter of the locked laser. The electrodes of the science chamber are compensating external electric fields, if the applied voltage has too much noise, this would heat up the atoms and can result in a linewidth broadening. For this reason keeping noise on the control signal at a minimum is crucial for this setup.

Former experiments have proofed that a computer aided control system is an excellent way of combining the required precision with a comfortable interface. More benefits arise from automation and the possibility to rerun settings from former measurements. The existing labview-based computer control software being used in various projects in our group could not be simply transferred to our setup due to hardware incompatibilities.

Additionally, while being very flexible already, the existing software does not contain all features we would like to have for this new experiment. This includes e.g. multiple parameter scanning, extensibility, continuous running.

4.2 Hardware

As the existing experiment shows, working with ultracold Rydberg atoms results in two distinct timescales, on which parts of the experiment have to be operated. The first time regime is on the time scale of 10 µs, which consists of the magneto-optical trap and the transport.
Then there is the Rydberg excitation which takes place on an approximate 10 ns timescale. After excitation the Rydberg atoms have to be detected with the MCP or channeltron. To perform the measurement on the nanosecond timescale we are using a Pulseblaster card from Spincore. The implementation of the user interface and the characterization of this card is described in Udo Hermann's bachelor thesis [31].

For the 10 µs experiment control we use a National Instruments PXI system (NI PXIe-1078) with three analog output cards (NI PXI-6733), two digital output cards (NI PXIe-6535) and one analog input card (NI PXIe-6356). The PXIe-1078 is a modular system in which it is possible to plug in any kind of PXI compatible card. It provides a back-plane on which the trigger pulses and the clock signal can be distributed to each card.

The main reason to use this system was compatibility with the other groups working at the institute. Overall, the working experience with this system has been somewhat negative, due to various unexpected problems for this specific hardware combination. Although the chassis system includes various dedicated routes for synchronization of multiple I/O cards, National Instruments provides online examples for synchronizing specific hardware. However none of these examples worked for our hardware combination. Calling the support hotline did not help at all as they where referring to the online examples.
Finally a solution was found by reading through the whole DAQmx[1] application programming interface (API) finding a possibility to route the clock signals manually. In addition the routing tables of each I/O card had to be consulted to find out which card is capable of which synchronization method. With these information it became clear, that the only card with that all the others in this setup can be synchronized to, is the PXIe-6356. In the end this setup is up and running, but a last obscurity stays. To be able to synchronize both digital cards we had to change the synchronization from rising edge to falling edge. The National Instruments support hotline was not able to explain this behavior to us, again.

The analog I/O devices have a commercial adapter[2] to convert the 68-pin SCSI-II type connector to 8 BNC connectors. For the digital I/O devices we built two 4 RU[3] high cases with buffer cards, which amplifies the output current and pairwise decouples the

[1] National Instruments' I/O programming interface
[2] BNC-2110
[3] Rack unit

outputs galvanically.

4.2.1 Specifications

Amount	Card Type	Specifications
3	PXIe-6733	Analog Output 8 Analog Output Channels, Synchronizable 16 Bit Resolution per Channel Voltage: $-10 \ldots +10\,\mathrm{V}$ Current Drive Single: 5 mA Current Drive All: 40 mA Slew Rate: $15\,\mathrm{V/\mu s}$ Noise: $80\,\mu\mathrm{V}_{rms}$ DC to 1 MHz 8 TTL Ouput Channels, Synchronizable Buffer: 8192 Samples (Analog), 2048 Samples (Digital)
2	PXIe-6535	Digital Output 32 Digital Output Channels, Synchronizable Logic Level: 2.5 V & 3.3 V
1	PXIe-6356	Analog Input & Output 8 Analog Input Channels, Synchronizable 16 Bit Resolution per Channel Voltage: $-10 \ldots +10\,\mathrm{V}$ Timing accuracy: 50 ppm of Sample Rate Timing resolution: 10 ns Sampling Rate: max 1.25 MS/s per Channel 2 Analog Output Channels Current Drive Single: 24 mA Current Drive All: 576 mA Slew Rate: $20\,\mathrm{V/\mu s}$

4.2.2 Output Characterization

To validate the specifications some measurements have been performed. The first measurement was to verify the 16bit channel depth of the analog output cards. The minimal step size of the output voltage is given by $20\,\mathrm{V}/2^{16} = 0.3\,\mathrm{mV}$. The measurement was done using a Voltcraft VC920 which has a resolution of 0.1 mV. Figure 4.1 a) shows a nice compliance to the calculated expectation for the positive voltage range. The negative voltage range is not as clear (see figure 4.1 b) as the positive one. As this voltmeter is a relatively cheap one there is a possibility that the resolution for negative voltages might not be as good as for positive ones.

As shown in figure 4.2 the rise and fall time between $-10\,\mathrm{V}$ and $10\,\mathrm{V}$ has been measured

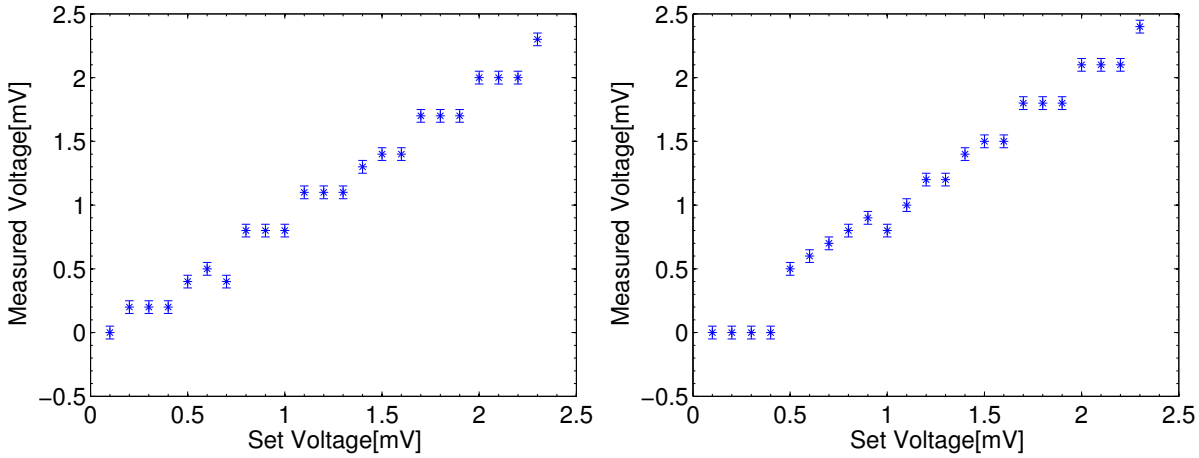

(a) 16bit resolution between 0 and 2.5 mV (b) 16bit resolution between 0 and −2.5 mV

Figure 4.1: Verification of 16bit resolution of a PXIe-6733 analog output card

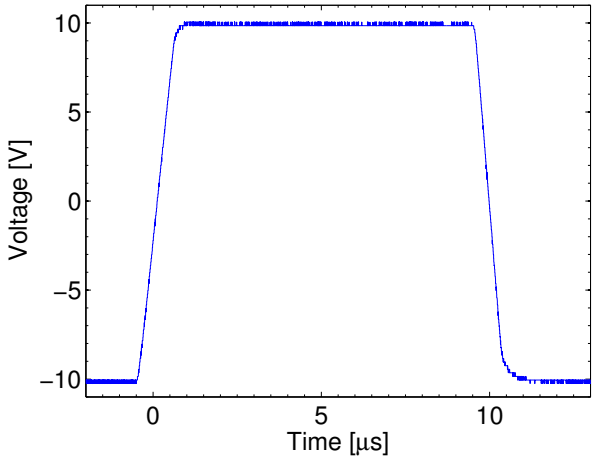

Figure 4.2: Rise time from −10 V to 10 V of the PXIe-6733

with an Agilent DSO-X 2004. After a linear fit to the slope the rise time from 10% to 90% of the final value is 1.009 µs and the fall time is 0.776 µs.

Talking about precision the jitter between two synchronized channels has been measured. Comparing two digital channels from different cards there is a little jitter given by the FWHM of 5.53 ns. This measurement has been done with the output buffers installed, each channel gets a 60 ns delay added due to the amplification. This can not be seen in this measurement as both channels are measured after the isolation box. All time resolution measurements have been done with a SensL HRMTime TDC with a resolution of 27 ps.

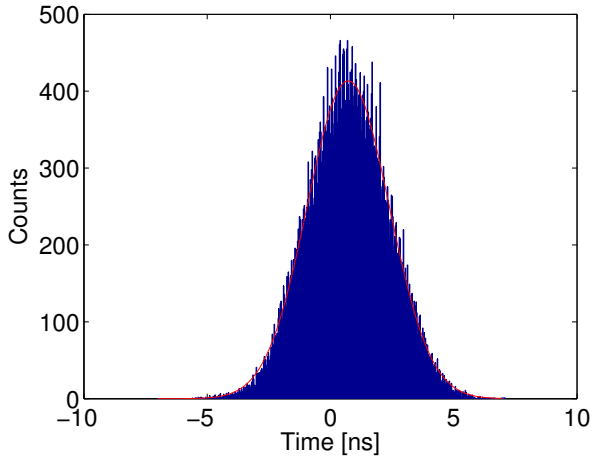

Figure 4.3: Jitter between two digital channels from different cards.

4.3 Software

Having specified the hardware, this chapter describes how the interaction between the user and the hardware is achieved. Therefore a software solution has been built as an interface between user and hardware. Accordingly, neither the visualization nor the extensibility should be a limiting factor. Another important fact is the maintainability of the created solution as it has to withstand generations of PhD students.
To minimize fluctuations in our measurements due to external temperature drifts, we decided to let the control system run continuously. By doing so we can ensure a constant noise at all time, which cancels out by averaging over a few runs. Whereas a start up phase adds a time dependent noise, which does not cancel out. Switching on and off the experiment every day, would cause a delay until measurement could start, since, after switching on the experiment needs some time to reach an equilibrium state. Measuring during this time would cause a time dependent noise from shot to shot.
For this reason the software must be capable of handling the output and the user input concurrently. A double buffering system (see the backend section 4.3.4) was created to accept the user input, validate it and if it is valid copy it to a backend which then will create the desired format for the output device.

4.3.1 Requirement Specifications

- Stability

  Being fault tolerant to wrong user input.

- Extensibility

  An easy possibility to extend the program to future needs.

- Performance

  Create a graphical user interface which reacts directly on the input.

- Concurrency

  Have a backend run concurrently to the frontend and handle the output with the National Instruments device.

- Synchronicity

  Having all output devices synchronized to one central clock.

- Storing

  Save data in a format which is human readable and reloadable.

4.3.2 Choosing a Programming Language

With the requirements specified a suitable programming language has to be found. The following chapter discusses a few candidates.

LabVIEW

As we are working with National Instruments devices it seems obvious to use LabVIEW. LabVIEW is a visual, data flow oriented programming language. This is quite a nice way to program simple measurement setups. However it is quite hard to build a flexible control system at this complexity using LabVIEW. The experience of former experiments has shown that it is possible to use LabVIEW, but the maintainability is getting worse over the years. Another important point is the achievable flexibility with this visual programming concept. The common way is to encapsulate the code in customized VIs, but this is very limiting and difficult to change afterwards. A VI is a graphical representation of a block of graphical code. Any program flow can be merged into a new block with defined input and output. Then the inputs and outputs are wired with lines which have a color for each type, though if one data type appears more often they all look the same. That makes it very easy to lose track of program flow. Knowing all that, LabVIEW was dismissed.

MATLAB

The next programming language often used in the scientific world is MATLAB. As MATLAB is a written (non visual) programming language the maintainability is much better than LabVIEW. It also has the possibility to create graphical user interfaces programmatically. Needing a continuously running control system the user interface has to run in parallel with the backend. As MATLAB has no possibility of running functions in parallel and the performance of the graphical user interface drops dramatically when too many elements are added. MATLAB was also not a suitable candidate for our control system.

C#

After looking at two candidates which did not fulfill the requirements C# [32], [33] was chosen. Its object-oriented programming style makes it easy to create flexible and maintainable code. Together with its perfect integration into Windows the creation of a well performing graphical user interface is possible. Furthermore it also supports multi-threading which makes the double buffer approach feasible.

4.3.3 Maintainability and Flexibility

This chapter describes programming techniques used to achieve a maintainable and flexible software design from the beginning.

Object Oriented Programming

Object oriented programming (OOP) is an approach to solve the problem of code redundancy [34]. It is an analogy to real world objects, which have attributes and functions. So an object in this programming language has attributes, that are like variables in a normal programming language like MATLAB, as well as functions, called methods, which are tied to that object. This makes them slightly different than the functions in MATLAB. A method in an object oriented language only works on the object it belongs to. That is quite different from a function in MATLAB where always some parameters are passed in to work with.
The redundancy of the code is reduced due to the fact that objects can inherit from each other. This is quite similar to inheritance in biology. For example everybody has a mother and father, where the son has inherited attributes from both mother and father. Creating abstract classes, from which more explicit classes can be derived, reduces code redundancy. Writing code just once makes a program even more stable as a bug has to be fixed only once. That is why this concept is so common nowadays.

Model-View-Controller

Design patterns [35] are generic solutions to common problems and one, namely the model-view-controller (MVC) pattern, was used in this project. A major goal of our software was to create it as stable as possible. This pattern is designed to build robust and extensible user interfaces.
Therefore it splits the program into three components, a model which represents the backend in the means of the data storage. Then there is the controller, that will handle all logic involved in the view (GUI). The third part is the view, which could be any kind of visualization e.g. website or GUI. This decouples the three components, as the model only has to exchange information with the controller and the view only communicates with the controller. Thereby the extensibility is accomplished by having two interfaces defined. That makes it possible to change everything inside of the model, view or controller as long as the interface between them is kept the same. For example the view can be switched to a website instead of the actual Windows Presentation Foundation (WPF) representation as long as it uses the same interface as the one before.

Threading

In computer science, a thread is the smallest unit an operating system, e.g. Microsoft Window or Linux can schedule. A thread runs inside of a process, which means if there are more than one thread running inside of one process they share the same memory space. This makes it comfortable to share variable or in general data between them. With this it is possible to run parts of a program in parallel. The parallelism is achieved on a single CPU machine by time-division multiplexing. Time-division multiplexing just divides the calculation time of one CPU into small pieces and distribute those pieces equally among the threads. On a multi CPU machine concurrent handling of threads is achieved by letting each CPU handle one thread. With threads it is possible to run the graphical user interface in parallel with the backend which manage the entered data e.g. stores them on the hard drive and generates the format for the National Instruments device.

4.3.4 Backend

Having found a suitable programming language the model for the MVC design pattern was designed. The focus during the design process was to built a flexible, extensible and fault tolerant backend. As stated before the experiment is running continuously. Also the double buffer has been implemented. With this it is possible to keep the heating of the electronic devices in an equilibrium. Accordingly, the generated noise of this heating is getting time independent and is canceled out by averaging over a few runs. As a result we gain an extra of a few hours of time for our measurement time, because there is no time lost to start up procedures. A schematic illustration of the double buffer approach

can be seen in figure 4.4.

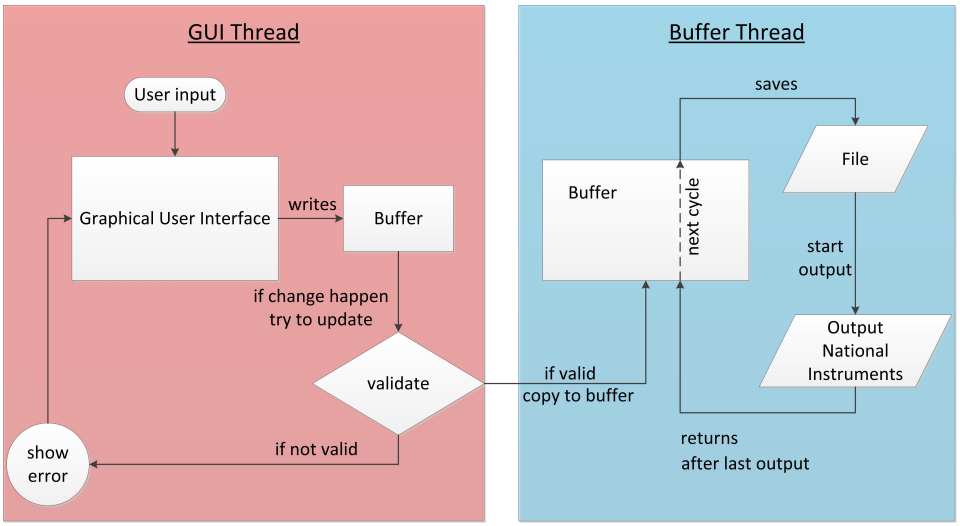

Figure 4.4: The flow of the program starting with the user input. After having validated the user input it is passed to the buffer thread which handles the output via the National Instruments device.

The program starts when a user inputs some run definitions in the user interface. This input is stored in the graphic buffer and then is checked for validation e.g. no entered value is out of range, no negative times. If the input passes this validation it is copied to a second buffer which is handled in a second thread. This buffer thread runs concurrently with the GUI thread and handles the output via National Instruments and subsequently stores the parameters to a hard disk (HDD). If an error occurs during validation the data is not copied to the buffer thread, but an error is shown to the user. The buffer thread then keeps on cycling with the last data-set it has in its buffer. All parameters of a cycle are stored on HDD for documentation purposes.

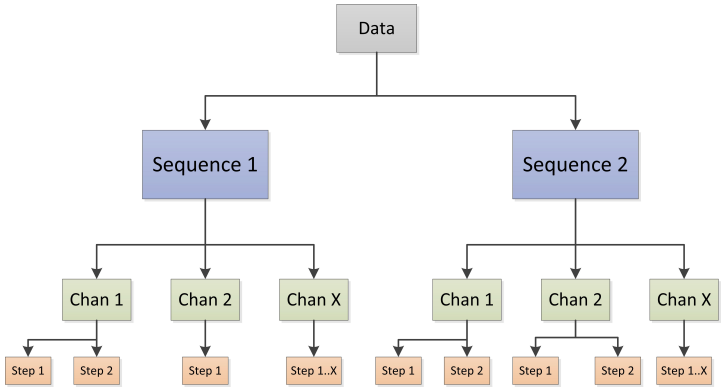

Figure 4.5: Internal data representation in a tree structure.

As the internal data structure is designed as a tree (see figure 4.5), it is easy to serialize[4] it to a disk. We save two versions, a human readable JavaScript Object Notation (JSON) file and a binary reloadable one.

We implemented the backend as a tree structure, since it gives us the most flexibility and extensibility. Starting at the top, there is data object which holds all information needed for one cycle. The next lower layer consists of sequences in which a run is split. Beneath each sequence are all channels, which hold the steps defined for this sequence. Each vertex is represented by an object in C# which has a multitude of attributes and methods to provide a simple way of extending them.

The API of DAQmx[5] requires a special format of input, to output the voltage signals. For digital output channels this format is a 1D array of a 32bit integer. This integer is a bit mask as every bit of the integer represents the status of a channel, where 1 means on and 0 indicates off. Each element in this array represents the action for a 10 µs step. The format for the analog channels is a 2D array of double[6] values. The order of the array is $8 \times n$ where the dimension of size 8 represents each channel of an analog card, the n represents the amount of 10 µs steps.
As one array keeps the information for one card and we are having three analog output cards and two digital output cards, we need two 1D integer arrays and three 2D double arrays.

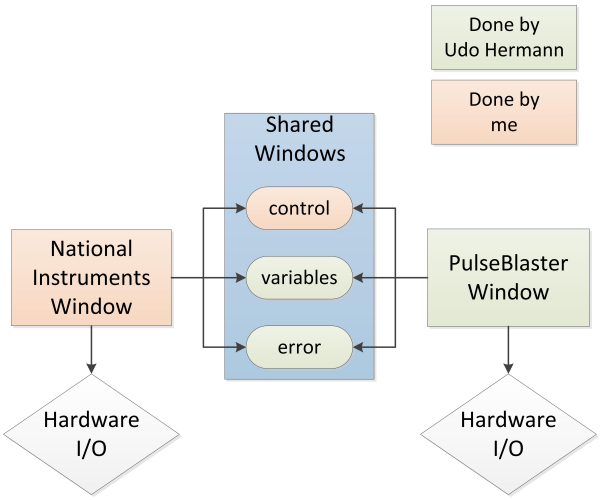

Figure 4.6: All windows the software has and who has built it.

[4]Serialization in computer science means to convert the actual data into a format which can be stored for example, in a file or memory buffer.
[5]National Instruments' API for I/O
[6]Floating point value of 64bit

Interaction between the windows

As the program has been developed in cooperation with Udo Hermann the diagram 4.6 shows which part is done by whom. Each hardware device has its own visual representation, but there are also windows and functionalities which are shared among the windows e.g. error output, variables and the main control window.

4.3.5 Graphical User Interface

Having an appropriate programming language and a working model, this chapter shows the implementation of the GUI as a view.

Channel Window

With our hardware being capable of 10 µs output time steps the backend of the software has to generate values for every output time step. We decided to represent every hardware device in a separate window to keep a lucid view. Such a channel window offers an easy and clear way to enter the values for an experiment cycle. As one experiment cycle can run up to one minute, lots of steps have to be defined. We introduced tabs to our user interface to bundle phases of the experimentation cycle to a logical unit. Each logical unit exists in every window to keep it clear what happens concurrently. In each tab the channels of a card are represented in rows. As we have decided to specify time as a relative value we were working with durations. Accordingly, each value entered for a channel has a duration and the absolute time has to be calculated by the computer.

As a result of this design concept we created the forms for a step which can be seen in figure 4.7a for analog channels and in figure 4.7b for digital channels.

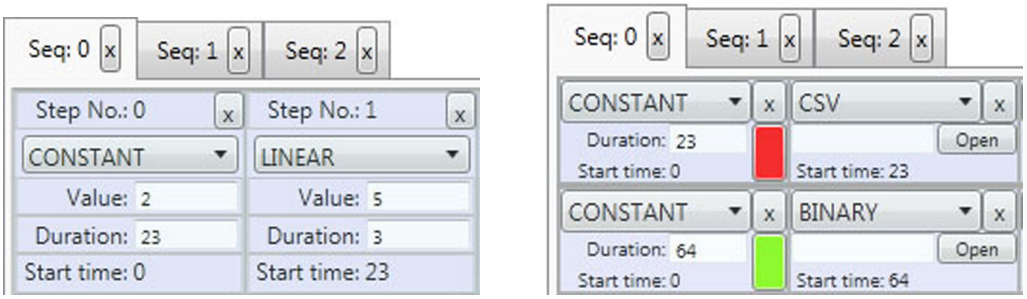

(a) Analog card window (b) Digital card window

Figure 4.7: Cutout of each window that represents an output device.

A step consists of a drop-down menu in which the type of step can be selected, for example constant value, different ramp types (e.g. linear, exponential) or loading calculated data sets. As each channel can contain an arbitrary amount of steps, the

duration for a tab is calculated from the longest channel in this tab. All the other channels will be filled with the last value set until they are equally long. If the second tab is added, then all its defined time steps will happen after the duration of the first tab. Therefore, each tab exists in every window and the duration of each tab is computed through all windows.

Sequence Window

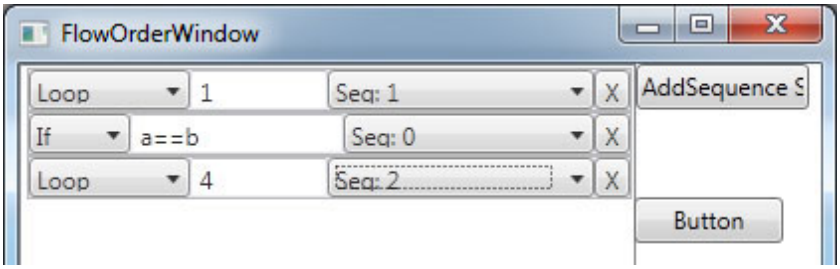

Figure 4.8: Sequence window

To have a more precise control possibility, an additional window was created (see figure 4.8) to order the flow of the tabs. In this window every row represents an order item i.e. loop or condition which can be selected from a drop-down menu . With this it is possible to loop a tab or only have it run under certain condition. The variables that can be used to define a condition can be any variable defined in the variable window.

Variable Window

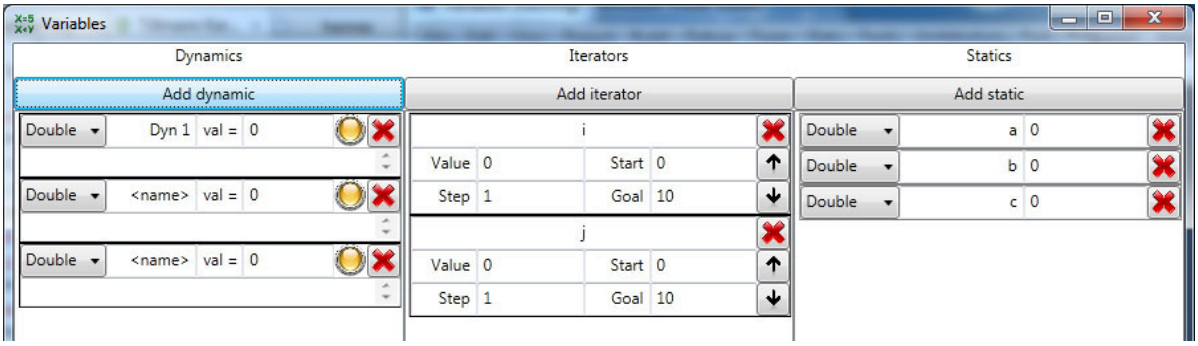

Figure 4.9: Variable window

To perform complex measurements, it is necessary to change parameters of the experiment from run to run. Therefore a variable window has been designed. As shown in figure 4.9 the window is divided into three parts. The most right part is for “static variables”. These make it easier to use an identical value more than once and keep it

clear what the value stands for, by giving it a name. They just map a variable name to a value, that can be used as a time or a value in any step. In the middle of the window are the iterator variables. There a start and stop value is defined as well as a step size by which the variable is increased every cycle. If more than one iterator is defined,they behave like nested loops. On the left of the window are the dynamic variables. These can be used to calculate non-linear iteration steps or load any kind of file. This is possible, because these variables are represented by a python script which is evaluated every run. The python script is capable of using the iterator and static variables of the control window.

4.3.6 Measurements

Running this implementation rises the question how long one run actually takes. For example defining a 30 s run it could be assumed that some additional time is needed to generate the data for the DAQmx API and upload it to the National Instruments chassis.
The time it takes for a whole experimentation cycle is shown in 4.10a. What can be seen is that the slope of the curve is a little bit greater than 1. This means that there is actually some additional time needed to perform the output. Figure 4.10b looks at this in more detail. There one can see that the most time is needed to upload the data to the chassis. Surprisingly the generation of the data-set does not take long at all, although up to 1.6 GB of data has to be generated for a 60 s run.

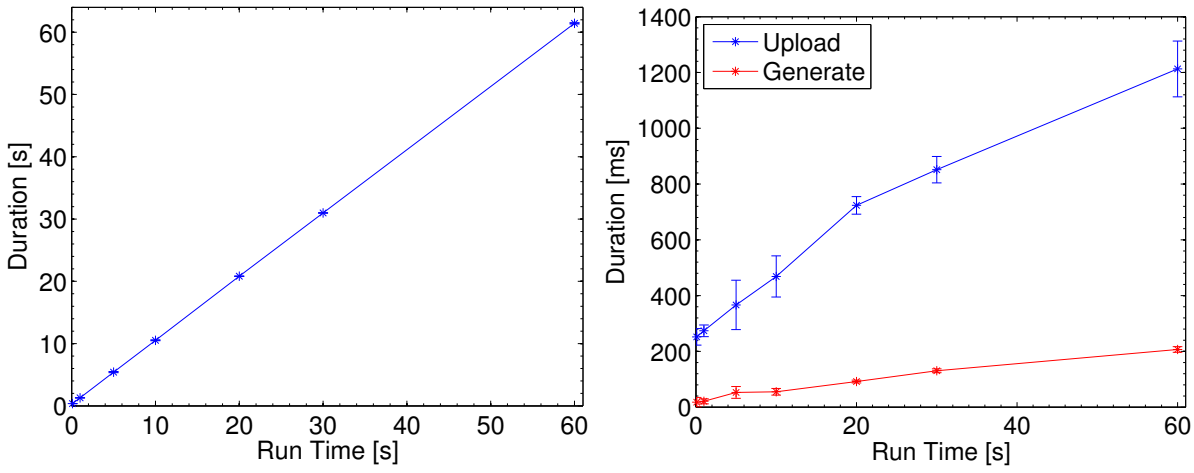

(a) Measurement of the real time duration over the defined output duration length of a whole run

(b) Measurement of the real time duration over the defined output duration length of the upload and generation process

Figure 4.10: Measurement of practical duration of an output cycle for different time length.

5 Summary and Outlook

The topic of this diploma thesis has been the set-up of a second generation cold Rydberg experiment. Especially the locking scheme, as well as the laser setup of the magneto-optical trap. Besides this a new computer aided control system has been built from scratch.
The diode lasers have been locked in a master-slave setup. In this setup the master laser is locked to an absolute frequency reference, to a DAVLL spectroscopy, respectively. This laser functions as a reference for the MOT lasers. The repumper and the cooler laser have been locked relative to this reference with a frequency offset lock. Therefore two beatnote boxes have been built. One at the frequency of 1 GHz for the cooler and one at 5.421 GHz for the repumper. With this versatile setup it is possible to scan each laser of about 1 GHz range. To determine the lock quality quantitatively we measured the the error signal while scanning the input frequency. Accordingly, looking at a spectrum analyzer we were able to see a small resonance of our beatnote of about a 200 kHz distance from the center locking frequency. As a result of the stabilization the line width of our lasers are < 40 kHz.
For stabilizing the lasers a PID controller has been developed. Being especially designed for our lasers this controller has been already used for other purposes, as its generic design allows the usage for other systems. Furthermore scientists from another institute have copied this design for their experiment, because of the high controlling bandwidth of up to 1 MHz.

The second topic covered in this thesis is the design of a new computer control system. During this work it has become obvious that a user interface should not be implemented with MATLAB or LabVIEW. Instead we headed for C# as a completely new approach in our institute to fulfill our requirements. This programming language is nicely integrated into windows and has a performance and functionality advantage over MATLAB and LabVIEW. With C# we implemented a visualization of one window per I/O card, which has an inner structure of tabs grouping experiment phases. To control the flow of these phases more precisely a flow control window has been added. This gives the opportunity to loop or run a phase under certain conditions. Furthermore, a window for defining variables has been added. These three types of variables cover all further needs to control scan parameters during a run cycle.

Combining these two parts, realized in this thesis, with the MOT setup it was possible to load atoms into the MOT (see figure 5.1). With this the first step towards a fully working experimental setup has been accomplished.

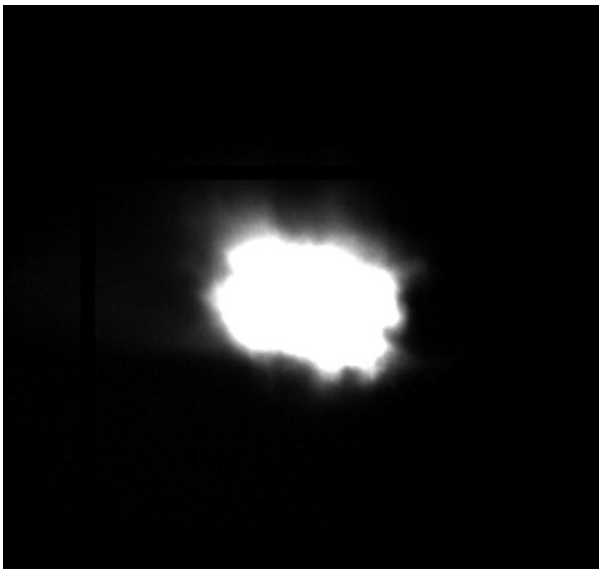

Figure 5.1: Trapped ^{87}Rb atoms

The next step towards a complete functional experiment is to load the cooled atoms into the magnetic trap and transport them into the Rydberg chamber. Therefore the transportation scheme has to be optimized to reduce the atom losses while moving them from the MOT to the experimentation cage. There the atoms are loaded into a QUIC-trap.

As proposed by H.P. Büchler [36] artifical "Superatoms" based on Rydberg atoms should have remarkable properties compared to normal atoms. With an induced dephasing the absorption of a single photon of a light field should be controllable.

In our first experiments we will try to build such a setup to investigate the properties of this promising proposal.

6 Appendix

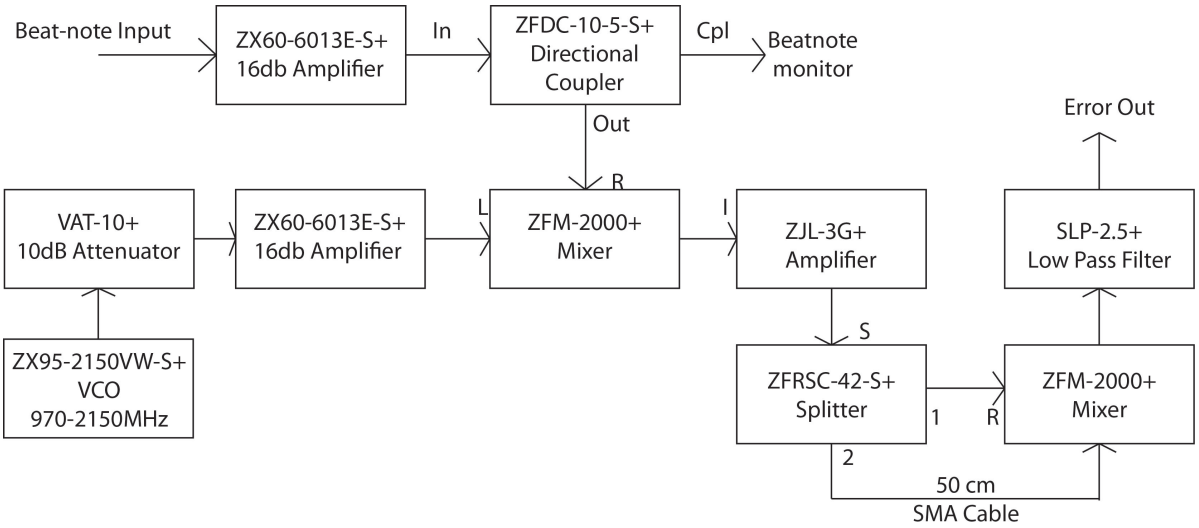

Figure 6.1: Schematic for a 1 GHz beatnote box built with Mini-Circuits components.

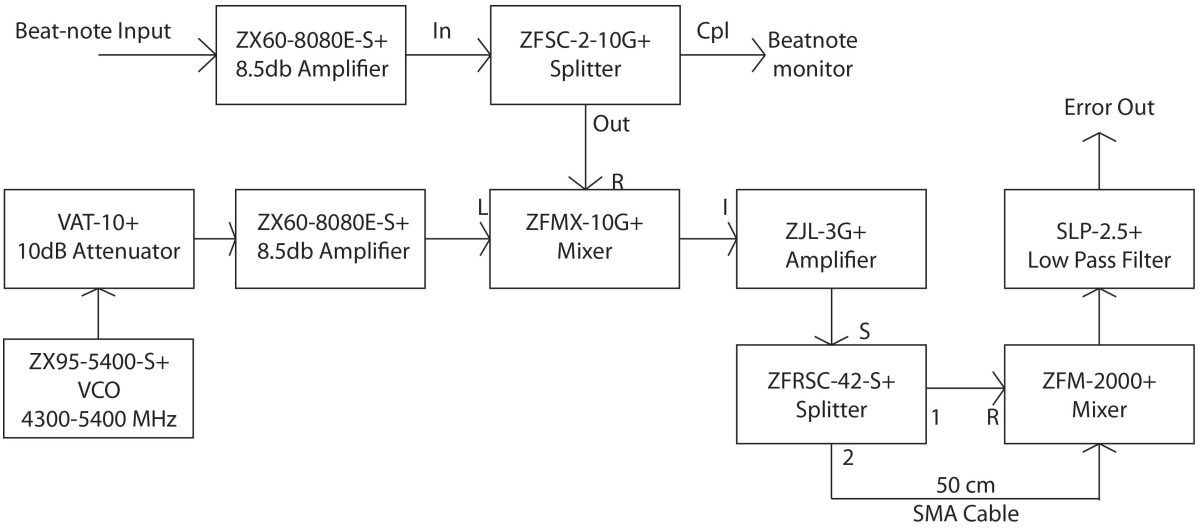

Figure 6.2: Schematic for a 5 GHz beatnote box built with Mini-Circuits components.

7 Bibliography

[1] M. Saffman, T. G. Walker, and K. Mølmer, "Quantum information with rydberg atoms," *Rev. Mod. Phys.*, vol. 82, pp. 2313–2363, Aug 2010.

[2] D. Jaksch, J. I. Cirac, P. Zoller, S. L. Rolston, R. Côté, and M. D. Lukin, "Fast quantum gates for neutral atoms," *Phys. Rev. Lett.*, vol. 85, pp. 2208–2211, Sep 2000.

[3] M. D. Lukin, M. Fleischhauer, R. Cote, L. M. Duan, D. Jaksch, J. I. Cirac, and P. Zoller, "Dipole blockade and quantum information processing in mesoscopic atomic ensembles," *Phys. Rev. Lett.*, vol. 87, p. 037901, Jun 2001.

[4] K. Singer, M. Reetz-Lamour, T. Amthor, L. G. Marcassa, and M. Weidemüller, "Suppression of excitation and spectral broadening induced by interactions in a cold gas of rydberg atoms," *Phys. Rev. Lett.*, vol. 93, p. 163001, Oct 2004.

[5] R. Heidemann, U. Raitzsch, V. Bendkowsky, B. Butscher, R. Löw, and T. Pfau, "Rydberg excitation of bose-einstein condensates," *Phys. Rev. Lett.*, vol. 100, p. 033601, Jan 2008.

[6] E. Urban, T. a. Johnson, T. Henage, L. Isenhower, D. D. Yavuz, T. G. Walker, and M. Saffman, "Observation of Rydberg blockade between two atoms," *Nature Physics*, vol. 5, pp. 110–114, Jan. 2009.

[7] A. Gaëtan, Y. Miroshnychenko, T. Wilk, A. Chotia, M. Viteau, D. Comparat, P. Pillet, A. Browaeys, and P. Grangier, "Observation of collective excitation of two individual atoms in the Rydberg blockade regime," *Nature Phys.*, vol. 5, pp. 115–118, 2009.

[8] T. Wilk, A. Gaëtan, C. Evellin, J. Wolters, Y. Miroshnychenko, P. Grangier, and A. Browaeys, "Entanglement of two individual neutral atoms using rydberg blockade," *Phys. Rev. Lett.*, vol. 104, p. 010502, Jan 2010.

[9] L. Isenhower, E. Urban, X. L. Zhang, A. T. Gill, T. Henage, T. A. Johnson, T. G. Walker, and M. Saffman, "Demonstration of a neutral atom controlled-not quantum gate," *Phys. Rev. Lett.*, vol. 104, p. 010503, Jan 2010.

[10] J. D. Pritchard, D. Maxwell, A. Gauguet, K. J. Weatherill, M. P. A. Jones, and C. S. Adams, "Cooperative atom-light interaction in a blockaded rydberg ensemble," *Phys. Rev. Lett.*, vol. 105, p. 193603, Nov 2010.

[11] Y. O. Dudin and A. Kuzmich, "Strongly Interacting Rydberg Excitations of a Cold Atomic Gas," *Science*, Apr. 2012.

[12] R. Löw, H. Weimer, U. Krohn, R. Heidemann, V. Bendkowsky, B. Butscher, H. P. Büchler, and T. Pfau, "Universal scaling in a strongly interacting rydberg gas," *Phys. Rev. A*, vol. 80, p. 033422, Sep 2009.

[13] V. Bendkowsky, B. Butscher, J. Nipper, J. P. Shaffer, R. Low, and T. Pfau, "Observation of ultralong-range Rydberg molecules," *Nature*, vol. 458, pp. 1005–1008, Apr. 2009.

[14] J. Nipper, J. B. Balewski, A. T. Krupp, B. Butscher, R. Löw, and T. Pfau, "Highly resolved measurements of stark-tuned förster resonances between rydberg atoms," *Phys. Rev. Lett.*, vol. 108, p. 113001, Mar 2012.

[15] T. Baluktsian, C. Urban, T. Bublat, H. Giessen, R. Löw, and T. Pfau, "Fabrication method for microscopic vapor cells for alkali atoms," *Opt. Lett.*, vol. 35, pp. 1950–1952, June 2010.

[16] R. Daschner, R. Ritter, H. Kübler, N. Frühauf, E. Kurz, R. Löw, and T. Pfau, "Fabrication and characterization of an electrically contacted vapor cell.," *Optics letters*, vol. 37, pp. 2271–3, June 2012.

[17] J. Sedlacek, A. Schwettmann, H. Kübler, R. Löw, T. Pfau, and J. P. Shaffer, "Quantum assisted electrometry using bright atomic resonances," 2012.

[18] H. Kubler, J. P. Shaffer, T. Baluktsian, R. Low, and T. Pfau, "Coherent excitation of Rydberg atoms in micrometre-sized atomic vapour cells," *Nature Photonics*, vol. 4, pp. 112–116, Jan. 2010.

[19] B. Huber, T. Baluktsian, M. Schlagmüller, A. Kölle, H. Kübler, R. Löw, and T. Pfau, "Ghz rabi flopping to rydberg states in hot atomic vapor cells," *Phys. Rev. Lett.*, vol. 107, p. 243001, Dec 2011.

[20] A. Kölle, G. Epple, H. Kübler, R. Löw, and T. Pfau, "Four-wave mixing involving rydberg states in thermal vapor," *Phys. Rev. A*, vol. 85, p. 063821, Jun 2012.

[21] S. Imanishi, U. Tanaka, and S. Urabe, "Frequency stabilization of diode laser using dichroic-atomic-vapor laser lock signals and thin rb vapor cell," *Japanese Journal of Applied Physics*, vol. 44, no. 9A, pp. 6767–6771, 2005.

[22] U. Schünemann, H. Engler, R. Grimm, M. Weidemüller, and M. Zielonkowski, "Simple scheme for tunable frequency offset locking of two lasers," *Review of Scientific Instruments*, vol. 70, no. 1, pp. 242–243, 1999.

[23] E. D. Black, "An introduction to Pound–Drever–Hall laser frequency stabilization," *American Journal of Physics*, vol. 69, no. 1, p. 79, 2001.

[24] C. Tresp, *Towards a two photon rydberg excitation.* Master thesis, Stuttgart University, November 2012.

[25] M. Greiner, I. Bloch, T. W. Hänsch, and T. Esslinger, "Magnetic transport of trapped cold atoms over a large distance," *Phys. Rev. A*, vol. 63, p. 031401, Feb 2001.

[26] T. Esslinger, I. Bloch, and T. W. Hänsch, "Bose-einstein condensation in a quadrupole-ioffe-configuration trap," *Phys. Rev. A*, vol. 58, pp. R2664–R2667, Oct 1998.

[27] R. Wanke, *Design and setup of an intensity and polarization stabilization system for diode lasers.* Bachelor thesis, Stuttgart University, August 2012.

[28] D. Stout and M. Kaufman, *Handbook of operational amplifier circuit design.* McGraw-Hill, 1976.

[29] H. Metcalf and P. Van Der Straten, *Laser Cooling and Trapping.* Graduate Texts in Contemporary Physics, Springer, 1999.

[30] D. A. Steck, "Rubidium 87 d line data," 2010.

[31] U. Hermann, *A nanosecond-resolution computer control system for determinstic excitation of Rydberg superatoms.* Bachelor thesis, Stuttgart University, August 2012.

[32] J. Richter, *CLR Via C#, Second Edition.* Redmond: Microsoft Press, 2006.

[33] J. Skeet, *C# in Depth.* Manning Pubs Co Series, Manning Publications, 2010.

[34] M. Weisfeld, *The Object-Oriented Thought Process.* Addison-Wesley Professional, 3rd ed., 2008.

[35] E. Gamma, R. Helm, R. Johnson, and J. M. Vlissides, *Design Patterns: Elements of Reusable Object-Oriented Software.* Addison-Wesley Professional, 1 ed., 1994.

[36] J. Honer, R. Löw, H. Weimer, T. Pfau, and H. P. Büchler, "Artificial atoms can do more than atoms: Deterministic single photon subtraction from arbitrary light fields," *Phys. Rev. Lett.*, vol. 107, p. 093601, Aug 2011.

Acknowledgements

I would like to express my gratitude to the people who were supporting me during this thesis.

First of all I would like to thank Prof. Dr. Tilman Pfau for giving me the opportunity to be part of this very interesting project.

Thanks to Huan, Christoph, Michael and Hannes for all the fun we had in the lab.

Special thanks to Dr. Sebastian Hofferberth as he was my supervisor and helped where ever he could.